











ORIGINAL RESEARCH

Nephronectin Is Required for Vascularization in Zebrafish and Sufficient to Promote Mammalian Vessel-Like Structures in Hydrogels for Tissue Engineering

Chinmoy Patra , PhD; Amey Rayrikar , PhD; Ganesh Wagh , MSc; Florian Kleefeldt , MD; Kaveh Roshanbinfar , PhD; Florian Cop, PhD; Iva Nikolic , PhD; Mirko H. H. Schmidt , MD, PhD; Amparo Acker-Palmer , PhD; Süleyman Ergün , MD; Felix B. Engel , PhD

BACKGROUND: Organs and tissues need to be vascularized during development. Similarly, vascularization is required to engineer thick tissues. How vessels are formed during organogenesis is not fully understood, and vascularization of engineered tissues remains a significant challenge.

METHODS AND RESULTS: Here, we show that the extracellular matrix protein nephronectin is required for vascularization during zebrafish development as well as adult fin regeneration and is sufficient to promote mammalian vessel formation and maturation. Nephronectin morphants and mutants exhibit diminished axial vein sprouting and posterior intersegmental vessel growth. Notably, the angiogenesis-associated integrins *itgav* and *itgb3.1* are coexpressed with nephronectin in the region of the caudal vein plexus and posterior somites; nephronectin binds to integrin alpha-V/integrin beta-3.1 (ITGAV/ITGB3.1), and *itgav* morphants phenocopy nephronectin mutants. In addition, nephronectin mutants showed decreased vessel maturation compared with wild-type siblings during caudal fin regeneration in adult zebrafish. Moreover, nephronectin promotes mammalian endothelial cell migration and tube formation in 2D and 3-dimensional in vitro tissue culture. Further, nephronectin enhances vascular endothelial growth factor-induced periaortic vascular capillary interconnectivity, vessel diameter, and vessel stability.

CONCLUSIONS: Collectively, our results identify nephronectin as a proangiogenic factor during embryonic development, which can be used to improve the vascularization of engineered tissues.

Key Words: extracellular matrix ■ nephronectin ■ tissue engineering ■ vascularization ■ zebrafish

Angiogenesis is defined as the formation of new lumenized functional vessels from preexisting blood vessels and starts with the specification of highly proliferative stalk cells and migratory leading edge tip cells.¹ Stalk cell proliferation and tip cell migration lead to the formation of vessel sprouts, which

subsequently interconnect with each other forming a lumenized vessel.^{2,3} Finally, these lumenized vessel networks undergo a remodeling process involving endothelial cell (EC) apoptosis, cell retraction, sprouting, and stabilization of connected vessels.⁴ During sprouting, tip cells lead each sprout through extending

Correspondence to: Chinmoy Patra, PhD, Department of Developmental Biology, Agharkar Research Institute, G.G. Agarkar Road, 411 004 Pune, India. Email: cpatra@aripune.org and Felix B. Engel, PhD, Experimental Renal and Cardiovascular Research, Department of Nephropathology, Institute of Pathology and Department of Cardiology, Friedrich-Alexander-Universität Erlangen-Nürnberg (FAU), Kussmaulallee 12 (TRC), 91054 Erlangen, Germany. Email: felix.engel@uk-erlangen.de

Amey Rayrikar is currently located at the Division of Basic and Translational Cardiovascular Research, Department of Cardiology, Boston Children's Hospital, 300 Longwood Avenue, Boston, MA 01225, USA.

This article was sent to Daniel T. Eitzman, MD, Senior Guest Editor, for review by expert referees, editorial decision, and final disposition.

Supplemental Material is available at <https://www.ahajournals.org/doi/suppl/10.1161/JAHA.123.037943>

For Sources of Funding and Disclosures, see page 17.

© 2025 The Author(s). Published on behalf of the American Heart Association, Inc., by Wiley. This is an open access article under the terms of the [Creative Commons Attribution-NonCommercial-NoDerivs](#) License, which permits use and distribution in any medium, provided the original work is properly cited, the use is non-commercial and no modifications or adaptations are made.

JAHA is available at: www.ahajournals.org/journal/jaha

RESEARCH PERSPECTIVE

What Is New?

- This study shows that the extracellular matrix protein nephronectin is required for angiogenesis during embryogenesis and tissue regeneration.
- In vivo and in vitro data indicate that nephronectin is a proangiogenic factor suitable to enhance vascularization in tissue engineering.

What Question Should Be Addressed Next?

- In the future, it will be important to elucidate downstream signaling mechanisms through which nephronectin promotes angiogenesis as well as to implement nephronectin in approaches to engineer thick tissues to contribute to the development of novel potential therapeutic interventions in regenerative medicine.

Nonstandard Abbreviations and Acronyms

AV	axial vein
CVP	caudal vein plexus
DLAV	dorsal lateral anastomotic vessel
DV	dorsal vein
EC	endothelial cell
ECM	extracellular matrix
hpf	hours post fertilization
HUVEC	human umbilical vascular endothelial cell
ISV	intersegmental vessel
mr-NPNT	recombinant mouse nephronectin
TALEN	transcription activator-like effector nuclease
V/V	volume/volume
VV	ventral vein
W/V	weight/volume

long filopodia and migrating in response to angiogenic cues.¹ In contrast, stalk cells have fewer filopodia but are proliferative, adding new cells at the base of the sprout, promoting sprout growth and vessel lumenization. This process is regulated by fine-tuning between proangiogenic and antiangiogenic molecules; present on the cell surface or in the extracellular matrix (ECM).⁵ Several signaling cues regulate tip and stalk cell specification, including Dll4/Notch^{6–8} and Wnt-frizzled⁹ signaling. Vessel sprouting is promoted by VEGF (vascular endothelial growth factor),³ BMP (bone morphogenetic protein),¹⁰ and Unc5b-netrin.¹¹ In contrast,

angiogenesis and vessel remodeling are negatively regulated by semaphorin-plexins/neuropilins¹² and ephrin-Eph,^{13,14} respectively.

The ECM was long considered an inert scaffold material to provide tissue stability. However, recent studies suggest that besides providing mechanical support, the ECM is a hub of active growth factors essential to modulate cell signaling during organ growth, maintenance, and repair.^{15–17} It has, for example, been shown that the ECM molecule MAGP-2 (microfibril-associated glycoprotein)-2 regulates angiogenesis by regulating notch signaling.^{18–20} A number of other ECM molecules have been identified that inhibit (eg, endostatin, decorin, and thrombospondin-1 and -2)^{21–24} or promote (fibrillin-1,²⁵ fibulin-1,²⁶ fibronectin,^{27,28} laminins,²⁹ perlecan,³⁰ tenascins,^{31,32} collagens,³³ and vitronectin^{34,35}) angiogenesis by inducing EC proliferation, migration, or vessel stabilization.

NPNT (nephronectin) is an ECM molecule consisting of an N-terminal signal peptide followed by several EGF (epidermal growth factor)-like repeats, an arginine-glycine-aspartic acid sequence, and a C-terminal MAM (meprin, A-5 protein, and receptor protein-tyrosine phosphatase mu) domain. Thus, NPNT is a member of the EGF-like protein family. It was first identified in mouse kidneys as a ligand of integrin $\alpha 8 \beta 1$ ³⁶ that is required for kidney morphogenesis^{37,38} and differentiation of mesenchymal cells to smooth muscle cells at the hair follicle bulge in mice.³⁹ We have shown that *npnta*, encoding NPNT a, a zebrafish ortholog of mammalian NPNT, is expressed in the developing zebrafish heart, where it regulates endocardial cell differentiation during valve formation.⁴⁰ Subsequently, it has been shown that mr-NPNT (recombinant mouse NPNT) promotes cardiomyocyte attachment, sarcomere maturation, and alignment through its integrin-binding arginine-glycine-aspartic acid motif.⁴¹ Nephronectin also inhibits cell migration in malignant carcinoma,⁴² promotes osteoblast differentiation in vitro,⁴³ and instructs selective synaptic choice from distinct retinal ganglion cells to wide-field neurons.⁴⁴

In regard to angiogenesis, it has been reported that mr-NPNT enhances a simian virus 40-transformed mouse microvascular endothelial cell line⁴⁵ and human umbilical vascular endothelial cell (HUVEC)⁴⁶ migration in 2-dimensional as well as branching and tube formation. In addition, mr-NPNT-induced vessel outgrowth from metatarsals but was less efficient than VEGF.⁴⁵ However, the physiological role of NPNT, for example, in vessel growth and stability, has not been reported.

Understanding angiogenesis is important for tissue engineering. Organ dysfunction and failure represent a major socioeconomic burden. Underlying diseases, such as myocardial infarction, can usually be treated only symptomatically. Therefore, there is great interest in establishing novel therapeutic strategies to prevent or reverse organ damage. Currently, the only available

therapy to reverse organ damage is organ transplantation. However, there is a severe shortage of donor organs.⁴⁷ Therefore, scientists focused on engineered tissues to replace diseased tissue to restore organ function. Although significant progress has been made in tissue engineering, the vascularization of engineered tissues is considered one of the major bottlenecks in the field. Without proper vascularization, tissues are limited in survival, as a steady supply of oxygen and nutrients cannot be achieved. Although engineered tissues become vascularized upon in vivo implantation, this process is often too slow to ensure survival of the implanted tissue. Therefore, large efforts are invested to establish strategies to guarantee tissue survival including promoting endogenous vascularization, using antiapoptotic or oxygen releasing materials to extend the time for endogenous vascularization, and providing prevascularization.⁴⁸ Although VEGF is often used to stimulate vascularization, it is now well known that VEGF induces only immature vessels.⁴⁹ Thus, it is important to identify novel regulators of vessel formation and stabilization that are applicable for tissue engineering approaches.

In this study, we assessed the role of NPNT in angiogenesis in early zebrafish development, the formation and stabilization of capillary-like sprouts in HUVECs, aortic ring assays, and tube formation in 3-dimensional (3D) collagen-I-based hydrogels. Our loss-of-function studies show that in zebrafish, *npnta* is required for posterior intersegmental vessel (ISV) growth, posterior axial vein (AV) sprouting during caudal vein plexus (CVP) formation, and ventral vein (VV) morphogenesis in embryos and vessel maturation during caudal fin regeneration in adults. In addition, mr-NPNT augments mammalian vascular growth and stability and enhances VEGF-induced angiogenesis. mRNA expression, loss-of-function, and interaction assays indicate that the effect of NPNT in vessel growth and stabilization is mediated through interaction with integrin $\alpha\beta3$. Finally, integration of NPNT into collagen-I-based hydrogels resulted in advanced tube formation and stabilization.

METHODS

The authors declare that all supporting data are available within the article (and its online supplementary files).

Zebrafish Maintenance

All procedures followed were in accordance with institutional guidelines. Wild-type AB and transgenic *Tg(fli1:EGFP)* and *Tg(etv2:EGFP)* zebrafish (*Danio rerio*) were housed in a state-of-the-art aquarium and maintained at 28 °C as described (Westerfield, 1993).⁵⁰

Reverse Transcriptase Polymerase Chain Reaction

RNA was extracted from pooled wild-type or morpholino injected embryos 2 days post fertilization, using Trizol (Invitrogen) according to the manufacturer's instructions. Using random hexamer and superscript III reverse transcriptase (Invitrogen), 1 µg of total RNA was subjected to cDNA synthesis. Quantitative reverse transcription polymerase chain reaction (PCR) was performed in a StepOnePlus Real-Time PCR Detection System (Applied-Biosystems) using Power SYBR Green PCR Master Mix (Applied-Biosystems) following standard protocols. Primers (5' to 3') for 18s ribosomal RNA, Fwd, TCGCTAGTTGGCATCGTTTATG and Rev, CGGAGGTTCCAAGACGATCA; *npnta* F1, ATGTGGATCATAAAGTTCATGTTGA; F2, CATTGGGAGCTTCAAGTGT; R1, CTTGCATCCGTGCTGACATA; R2, TCATCCACATCCACACAGGT were used. Gene mRNA expression levels were calculated relative to 18s ribosomal RNA using the ΔCt method. All reactions were run in triplicate.

In Situ Hybridization

Melanin pigmentation was stopped by adding 1-phenyl-2-thiourea (0.2 mM) to the embryo medium between 24 and 28 hours post fertilization (hpf). Paraformaldehyde fixed (4% in PBS [volume/volume (V/V)]) for overnight at 4 °C embryos were washed with (0.1% Tween 20 in PBS [V/V]) and processed for RNA in situ hybridization using digoxigenin-labeled riboprobe against *npnta*,⁴⁰ *itga8*,⁴⁰ *itgav*,⁵¹ and *itgβ3.1*.⁵¹ For histological analysis, whole-mount in situ hybridized embryos were embedded in gelatin (17% in PBS [weight/volume (W/V)]) and fixed overnight at room temperature (RT) with 4% paraformaldehyde in PBS (W/V), sectioned (40 µm) with a vibratome (Leica), and mounted (Kaiser's glycerol gelatin, Merck) on glass slides for microscopy.

Microinjection

Capped full-length *npnta* mRNA was synthesized after linearization (pCS2+/-*Fnnpnta*, SacII) using the mMACHINE SP6 in vitro Transcription Kit (Ambion) according to the manufacturer's instructions. Spliced blocking morpholino against *npnta* (MO2, 5-TGTGAAACGGCAGACGGAACTCACT-3) was injected into the cell at 1-cell stage embryos (≤ 2 nL; PV820 Injector, World Precision Instruments) with/without capped *npnta* mRNA in 0.1 M KCl.⁴⁰ Same volume 0.05% Phenol Red (V/V, Sigma) was injected as a control.

Generation of *Npnta* Mutant Zebrafish

All procedures followed were in accordance with institutional guidelines. Transcription activator-like effector

nuclease (TALEN) was used to generate the mutant allele. TALEN constructs for left and right arms were designed to target exon 4, with 18 and 16 base pairs long repeat-variable di-residue binding sequence and a 15 base pair long spacer; left arm sequence: GCGTGGGACCCAACAAAT; right arm sequence: GTTATACAGGAAAAAC. Left and right arm TALEN pair constructs were generated with the help of the Golden Gate TALEN assembly strategy. TALEN mRNAs were synthesized using an in vitro message machine kit (Invitrogen) following manufacturer instructions. Then, 200 pg mRNA of each arm was injected into 1-cell stage eggs to generate mutants. Injected eggs were raised and screened for germline transmission. Indel detection at the target locus was performed by high-resolution melting curve analysis of the genomic DNA isolated from the caudal fins of adult F1 animals. Indels were analyzed by sequencing the PCR amplified product using a primer; forward, GATGCAAGCACGGAGAATG; reverse, CCTTGGTTGCATGTTTTTCC, binding to the flanking region of the TALEN target. The allele (referred to as *npnta*⁻), harboring a 10-nt deletion, was selected and used in this study. Quantitative PCR was performed to detect the *npnta*⁻ allele (ari3) from genomic DNA.

5-Bromo-2'-Deoxyuridine Incorporation Assay

For 5-bromo-2'-deoxyuridine labeling, dechorinated 24 hpf control- or MO2-injected embryos were kept in embryo water containing 50 µg/mL 5-bromo-2'-deoxyuridine for 8 hours. Embryos were fixed in 4% paraformaldehyde in PBS (V/V) overnight at 4°C. The next day embryos were washed several times with 1X PBS and treated with 2N HCl in PBS for 1 hour at 37°C. Embryos were permeabilized and incubated with primary antibodies (rat anti-5-bromo-2'-deoxyuridine, 1:200 [Abcam]; and rabbit anti-GFP, 1:400 [Novus Biologicals]) for overnight at 4°C after a blocking step of 1 hour with a blocking solution (5% goat serum and 0.2% Tween 20 in PBS). Primary immune complexes were detected by Alexa 555- or Alexa 647- conjugated antibodies (1:400; Molecular Probes). Optical sections were captured with a Leica SP8 confocal laser scanning microscope.

Blood Vessel Growth Analysis During Caudal Fin Regeneration in Adult Zebrafish

All procedures followed were in accordance with institutional guidelines. One-year-old wild-type and *npnta* mutant zebrafish in a *Tg(etv2:EGFP)* background were used to study the neo-vessel growth in adults. EGFP expression in endothelial cells allows the study of blood

vessel growth during caudal fin regeneration. The same size of caudal fin tissues of wild-type and *npnta* mutants were amputated with a straight cut along the dorsal-ventral axis from the proximal part of the caudal fin using a razor blade after anesthetizing the animals for 5 minutes in 0.02% MS-222 (W/V, also known as Tricaine). Afterwards, animals were maintained in the zebrafish housing system. To analyze the degree of fin regeneration and blood vessel growth, caudal fin amputated animals at 5 days post amputation were anesthetized in 0.02% MS-222 (W/V). Regenerating fin tissues and blood vessels were imaged using a Nikon SMZ25 stereomicroscope. The area covered by the middle fin ray along with 2 ventral and 2 dorsal fin rays from the middle was selected for analysis. For fin regeneration, the length of the regenerated tissue was measured at 5 different places for each fin/fish and the average of these values was used for comparative analysis. Similarly, to explore the degree of nascent blood vessel growth, the length of the neo-blood vessel plexus along the mentioned 5 fin rays was measured, and the mean value was used for comparative analysis. To explore the degree of plexus remodeling into a matured vessel network in the proximal regenerated area, we analyzed the length of the matured vessel in the proximal region and the nascent vascular plexus in the distal tip of the aforementioned 5 fin rays. The mean value was used for comparative analysis. The measurement was done using FIJI software and statistical analysis was performed by GraphPad Prism 8 software.

Confocal Microscopy and Morphological Analysis

For whole-mount confocal microscopy, immunostained or anesthetized embryos (with 0.04% tricaine [W/V]) were mounted in 0.5% low-melting-point agarose (W/V) in E3 medium. Optical sections of the caudal vein plexus forming region were imaged with a Zeiss LSM710 or Leica SP8 confocal microscope. Images were processed with the help of LSM Image Browser, Zeiss, or Leica LAS AF Lite software.

Ethynyl-2'-Deoxyuridine Incorporation Assay

HUVECs were obtained from patients after the subjects gave informed consent, and the study was approved by the institutional ethics review committee at the Friedrich-Alexander-Universität Erlangen-Nürnberg under protocol number 374_20B. Glass coverslips (Ø 10mm) were first UV-sterilized for 30 minutes at room temperature in a cell culture hood in 24 well plates before they were coated with either sterile-filtered (0.22 µm) gelatin (1% in DPBS) or NPNT (R&D Systems,

USA, 10 µg/mL in DPBS) solution for 2 hours at 37 °C. Excess coating liquid was aspirated just before seeding cells. HUVECs from passage 2 were dissociated by adding 5 mL Triple and incubation at 37 °C for 5 minutes. After counting using an automated cell counter (Countess 3, ThermoFisher Scientific), the cells were seeded at 30 000 cells/well in endothelial cell growth medium (PromoCell, C-22010) onto freshly coated glass coverslips. Cells were left in culture overnight at 37 °C and 5% CO₂. Then, the medium was changed and HUVECs were cultured in endothelial cell basal medium (C-22210) + supplement with or without serum (PromoCell SupplementPack with individual media components, C-39210, minus serum, C-37320) containing 30 µM ethynyl-2'-deoxyuridine (1.5 mL medium per well). After 4 hours of ethynyl-2'-deoxyuridine incorporation, HUVECs were fixed in 4% paraformaldehyde and stained for ethynyl-2'-deoxyuridine and 4',6-diamidino-2-phenylindole using the Click-it EdU AlexaFluor 488 HCS kit (C10351, ThermoFisher Scientific) according to the manufacturer's instructions.

Cell Migration Experiment

Primary HUVECs (Lonza, Switzerland) were grown and maintained in endothelial cell Bullet Kit supplemented EBM-2 Basal Medium (Lonza). For cell migration assay 24-well tissue culture plates were coated with either 1% gelatin (control) or mr-NPNT in PBS (10 µg/mL) for 2 hours at 37 °C and the solution aspirated immediately before the cell plating. HUVECs from passages 3 to -5 were plated with EBM-2 Basal Medium supplemented with Bullet Kit, 100 µg/mL streptomycin, and 100 U/mL penicillin at the cell density of 30 000 per well. After reaching to near confluence, HUVECs were serum starved overnight, and wounding was done by scratching the cell monolayer with a p200 pipette tip in a straight line. At 1 hour post wounding culture medium was replaced with a fresh serum-starved medium and imaged with a Leica inverted microscope to document the initial wound area. Images of the wound area were captured at 6 hours post wounding to study the cell migration. National Institutes of Health (NIH) Image J software was used to quantify EC migration.

Tube Formation Assay

The 96-well plates and p200 tips were kept at 4 °C for at least 1 hour to set the basement membrane matrix. mr-NPNT (R&D Systems, USA) or BSA were mixed with growth factor reduced basement membrane matrix (BD Biosciences) at the concentration of 10 µg/mL. BSA (control) or mr-NPNT supplemented growth factor reduced basement membrane matrix was pipetted into each well of a 96-well plate. Plates were incubated at 37 °C and 5% CO₂ for 30 minutes to solidify growth factor reduced basement membrane matrix. HUVECs

from passages 3 to 5 were seeded on the surface of the casted growth factor reduced basement membrane matrix of 2500 cells/well density and placed at 37 °C and 5% CO₂. Images were captured with a Leica inverted microscope at 4 and 22 hours post seeding. Data were analyzed with the help of NIH Image J software (Wayne Rasband; National Institutes of Health, USA).

Aortic Ring Assay

All experiments were carried out according to German regulations (Regierung von Unterfranken, Wuerzburg, Germany). Aortic ring assay was performed as described previously.⁵² In brief, aortae were freed from perivascular fat, cut into 1-mm ring segments, and incubated in the absence of serum for 24 hours/37 °C/5% CO₂ (Opti-MEM + GlutaMAX-I, Gibco, Thermo Fisher, Waltham, MA, USA; cat. 51985-026). Ring segments were embedded in 1 mg/mL collagen-I solution (Merck Millipore, Burlington, MA, USA; cat. 08-115). Aortic rings were cultured in Opti-MEM culture medium supplemented with 2.5% (V/V) fetal bovine serum (Biochrom GmbH, Berlin, Germany) with or without addition of 50 ng/mL VEGF (Pepro Tech, Rocky Hill, NJ, USA; cat. 450-32) or 10 µg/mL mr-NPNT (R&D systems, Minneapolis, MN, USA; cat. 4298-NP-050) for 7 days at 37 °C/5% CO₂. The medium was replaced on days 3 and 5. Phase-contrast images were taken using a Leica DM IL LED Fluo microscope (Leica Microsystems, Wetzlar, Germany; equipped with Leica DFC 3000G camera). For pericapillary pericyte/smooth muscle cell recruitment analysis, aortic ring assays were fixed in 4% paraformaldehyde in PBS (V/V) overnight on day 7 and embedded in Tissue-Tek (Sakura Finetek Europe B.V., AJ Alphen aan den Rijn; The Netherlands). Cross-cryosections were performed and stained using a Cy3 labeled mouse anti-α-smooth muscle actin antibody (Sigma; C6198; 1:100) and 4',6-diamidino-2-phenylindole. Images were captured using a Keyence BZ9000 microscope (Keyence, Neu-lsenburg, Germany). Sprouting distance, branch point density, maximum vessel diameter, and α-smooth muscle actin stained area were calculated using NIH ImageJ software 1.47. For maximum vessel diameter analysis, the average of 2 thickest vessel diameters was considered for each sample.

Transfections, Immunoprecipitations, Gel Electrophoresis, and Western Blots

HEK293T cells were transfected with construct encoding for Flag-tagged NPNT and ITGAV or ITGB3 integrin subunits using Lipofectamine 2000 Transfection Reagent (Invitrogen, USA) as per manufacturer's instructions. After 48 hours cells were lysed in ice-cold lysis buffer (50 mM HEPES [4-(2-hydroxyethyl)-1-piper

azineethanesulfonic acid, pH 7.4], 150mM NaCl, 10% glycerol, 1% Triton X-100 plus protease and phosphatase inhibitors). Following centrifugation at 16200g for 10 minutes, supernatants were subjected to immunoprecipitation with anti-Flag antibody (clone M2, Sigma, Munich, Germany) in the presence of 30 μ L of Immunosorb A (Medicago, Uppsala, Sweden) overnight at 4°C. The following day, immune complexes were loaded onto sodium dodecyl sulfate-polyacrylamide gels and transferred to nitrocellulose membranes (GE Watter & Process, Herentals, Belgium). The membranes were next incubated with primary antibodies including anti-Flag, anti-ITGAV (1:1000, clone Q-20, Santa Cruz Biotechnology, Santa Cruz, CA), and anti-ITGB3 (1:1000, clone H-96, Santa Cruz Biotechnology, Santa Cruz, CA) for 2 hours at room temperature. It was followed by incubation with horseradish peroxidase-conjugated antimouse or antirabbit antibody for 1 hour at room temperature. Immune complexes were visualized by chemiluminescence using luminol following the manufacturer's instructions (Santa Cruz Biotechnology, Santa Cruz, CA).

Tube Formation in 3D Hydrogels

Primary isolated HUVECs at passage 2 were cultured in an endothelial-specific culture medium (PromoCell) and passaged at 85% confluency. To generate the 3D constructs, HUVECs (7.5×10^6 cells) were re-suspended directly in the pregel solution of rat tail collagen-I (3.7 mg/mL, Advanced Biomatrix alone or containing 10 μ g/mL mr-NPNT, R&D Systems) and incubated at 37°C and 5% CO₂ for 30 minutes. The final 3D generated constructs were cultured in endothelial cell growth medium. At day 1 and day 4, constructs were fixed in 3.7% paraformaldehyde in PBS (V/V) and stained for endothelial-specific marker, mouse anti-CD31 (Abcam, 1:20), overnight at 4°C. Secondary antibody from donkey antimouse Alexa Fluor 594 (Invitrogen, 1:500) was incubated with the construct at room temperature for 120 min. DNA counterstaining was performed by incubating the constructs with 4',6-diamidino-2-phenylindole (Sigma) for 10 minutes. Subsequently, samples were mounted on glass cover slides and confocal images were acquired by Zeiss LSM 800 confocal microscope. Data were analyzed using NIH ImageJ 1.47 software and the Angiogenesis Analyzer plugin.

Statistical Analysis

Differences between groups were considered statistically significant when the *P* value was ≤ 0.05 . Statistical significance was determined for quantitative PCR, axial vein sprout frequency, EC proliferation, sprout formation, vessel complexity, and vessel morphology by a 2-tailed Student's *t* test when comparing 2 samples

and a 1-way ANOVA followed by a post hoc test when comparing more than 2 samples, using Prism7 software. Data are represented as mean \pm SEM. ns: $P > 0.05$; * $P \leq 0.05$; ** $P \leq 0.01$; *** $P \leq 0.001$; **** $P \leq 0.0001$.

RESULTS

Npnta Is Necessary for Axial Vein Sprouting and Intersegmental Vessel Growth

Alignment of the amino acid sequence of NPNT of different species together with a domain structure analysis revealed that NPNT is highly conserved among zebrafish, humans, and mice (Figure S1), suggesting that NPNT may have similar functions in these organisms. In situ hybridization detected *npnta* transcripts in the pronephric ducts (green arrowheads) and CVP forming region (green arrows) at 20 to 30 hpf (Figure 1A). Moreover, at 30 hpf *npnta* transcripts are visible in the ventral part of the posterior somites (orange arrows; Figure 1A).

In zebrafish, the CVP is formed around 26 hpf by angiogenic sprouting of the posterior AV.⁵³ A subset of angiogenic sprouts extends ventrally and forms an interconnected plexus, the CVP.¹⁰ Over time, the VV develops through the vascular remodeling of the CVP by a pruning process, resulting in a continuous vessel running in parallel to the AV, which remains connected by interconnecting vessels and is now called the dorsal vein (DV). Therefore, we sought to identify the role of *npnta* in AV sprouting and VV morphogenesis. MO-mediated gene knockdown strategy was applied to explore the role of NPNT in vascularization during embryonic development. Two splice-blocking MOs were used that have previously been published.⁴⁰ They target the splice donor site of exon E5 (*npnta*-MO2) or exon E1 (*npnta*-MO3; Figure 1B and 1C). Exon E3 is not present in wild-type zebrafish as previously reported.⁴⁰ Injection of 2.4 ng of *npnta*-MO2 or 7.5 ng of *npnta*-MO3 per embryo resulted in $75.33 \pm 4.93\%$ and $80.33 \pm 2.52\%$ knockdown of *npnta* mRNA at 2 days post fertilization (Figure 1D), respectively.

To determine VV morphogenesis, *npnta*-MO2 or -MO3 were injected into 1 cell-stage embryo from transgenic (*Tg(fli1:EGFP)*) animals, which express EGFP (enhanced green fluorescent protein) in ECs. Whole mount confocal microscopy of the lateral view at 48 hpf suggests that dorsal aorta diameter, ISV frequency from the dorsal aorta, and DV morphology in *npnta* morphants are comparable to their control siblings. However, VV morphogenesis was disrupted in *npnta* morphants (Figure 1E and 1F). This contrasts with wild-type embryos (control), in which the VV is developed as a continuous vessel in parallel to DV and *npnta*

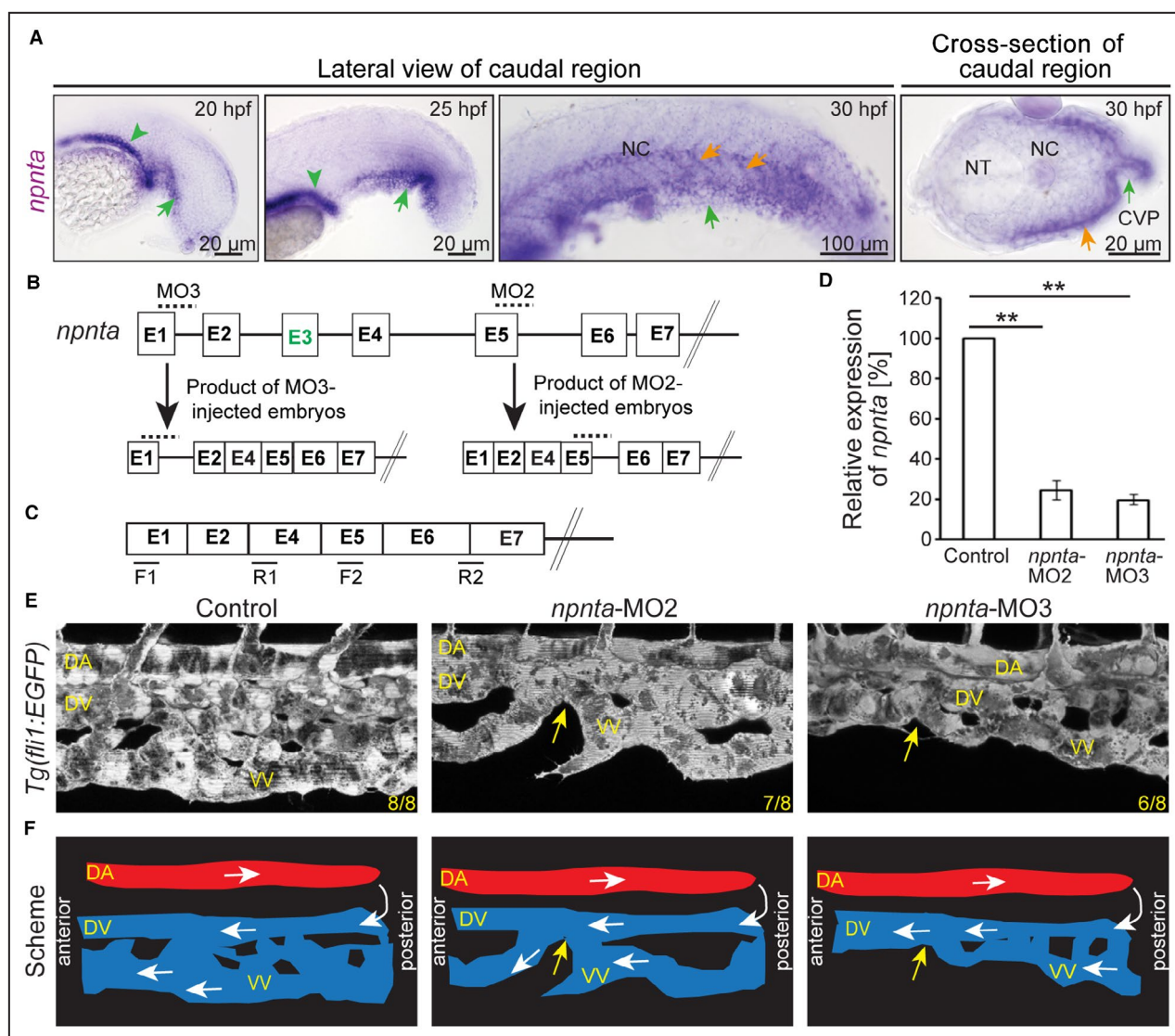


Figure 1. *npnta* knockdown disrupts ventral vein formation.

A, Representative brightfield images revealing *npnta* expression in zebrafish embryos based on whole-mount in situ hybridization. Green arrowheads: pronephros; green arrows: caudal vein plexus forming region; orange arrows: ventral region of the posterior somites. **B** and **C**, Scheme of the effect of MO2 and MO3. Boxes: exons. Lines: introns. Dotted lines in (**B**) indicate the region targeted by MO2 or MO3, and black lines in (**C**) indicate quantitative PCR primer positions to quantify stable matured *npnta* mRNA. Note, exon E3 is not used in wild types. **D**, Quantitative analysis of matured *npnta* mRNAs from control-, MO2- or MO3-injected zebrafish embryos at 30 hpf using *npnta* primers as indicated in (**C**) and 18S RNA primers (loading control; $n=3$, each sample is a pool of 40–50 embryos). Statistical significance was determined by 1-way ANOVA followed by a post hoc test. Data are means \pm SEM. ** $P\leq 0.01$. **E**, Lateral views of representative maximum projections of confocal images of the post-cloaca region from 48 hpf control-, MO2-, or MO3-injected *Tg(fli1:EGFP)* zebrafish embryos. Yellow arrows: discontinuation of VV. Numbers indicate the number of embryos with a phenotype vs the total observed embryos. **F**, Schematic depiction of (**E**). White arrows: blood flow. CVP indicates caudal vein plexus; DA, dorsal aorta; DV, dorsal vein; hpf, hours post fertilization; MO2,3 spliced blocking morpholino; NC, notochord; NT, neural tube; PCR, polymerase chain reaction; and VV, ventral vein.

morphants failed to develop a complete VV (Figure 1E and 1F).

Because VV development depends on the sprouting of the AV, we assessed the AV sprouting frequency and CVP morphology in wild-type embryos and *npnta* morphants during CVP formation at 28 hpf (AV sprouting), 33 hpf (formed CVP), and 40 hpf (formed VV). *Tg(fli1:EGFP)* single cell-stage embryos

were injected with *npnta*-MO2 or -MO3 and analyzed for sprouting frequency of the AV at 28 hpf. Maximum projections of the optical sections of the CVP forming regions showed abnormality in AV sprouting and CVP formation (Figure 2A). Quantitative analysis revealed that the sprouting frequency of the AV was significantly reduced in *npnta* morphants compared with control-injected embryos (control: 100 \pm 4.25%, MO2:

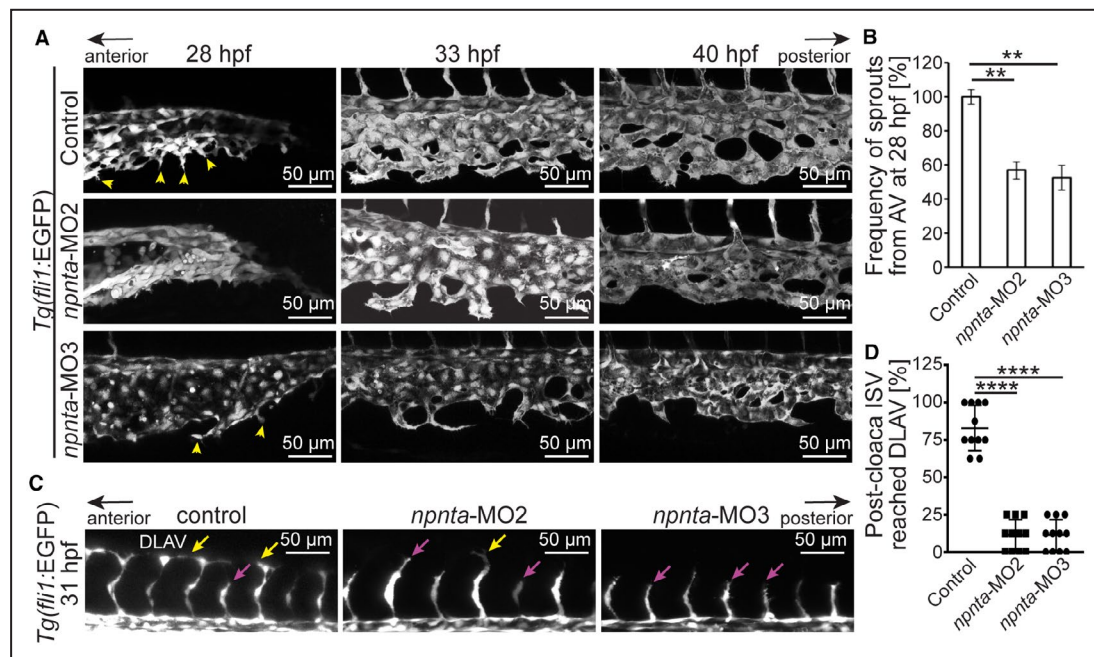


Figure 2. *npnta* knockdown disrupts axial vein sprouting and intersegmental vessel growth.

A, Lateral views of maximum projections of confocal images of caudal vein plexus of control-, *npnta*-MO2- or -MO3-injected *Tg(fli1:EGFP)* zebrafish embryos. Yellow arrowheads indicate ventral angiogenic sprouts at the axial vein. **B**, Quantification of angiogenic sprouts from AV at 28 hpf ($n=6$ embryos for each group). Mean angiogenic sprouts in the control embryos were considered as 100%. **C**, Maximum intensity projections of the confocal images of the lateral views of the post-cloaca caudal region show intersegmental vessels. Yellow arrows indicate ISVs that reached the dorsal lateral anastomotic vessel, and magenta arrows indicate ISVs that are yet to reach the DLAV. **D**, Quantification of how many of the 8 post-cloaca ISVs from each animal reached the DLAV at 31 hpf ($n=11$ embryos for each group). Pre-cloaca ISVs were not considered for analysis. Statistical significance was determined by 1-way ANOVA followed by a post hoc test. Data are mean \pm SEM. $^{**}P\leq 0.01$; $^{****}P\leq 0.0001$. AV indicates axial vein; DLAV, dorsal lateral anastomotic vessel; hpf, hours post fertilization; ISV, intersegmental vessel; and MO2,3 spliced blocking morpholino.

43.29 \pm 5.0%; MO3: 53.74 \pm 7.17%; **Figure 2B**), indicating *npnta* is necessary for AV sprouting. Further, because *npnta* transcripts are expressed in the ventral region of the posterior somites, we explored the ISV growth upon *npnta* knockdown. To explore ISV growth, 8 post-cloaca ISVs were analyzed. Whole-mount confocal microscopy of the post-cloaca caudal region at 31 hpf indicates that whereas in wild-type control embryos, around 80% of the 8 ISVs reached dorsal lateral anastomotic vessel (DLAV), in *npnta* morphants, most of the ISVs failed to reach DLAV (**Figure 2C** and **2D**). To validate the specificity of the *npnta* morphant phenotype, in vitro synthesized full-length *Danio rerio npnta* mRNA was coinjected with *npnta*-MO2 into single cell-stage *Tg(fli1:EGFP)* or *Tg(etv2:EGFP)* embryos, which express EGFP in ECs and quantified the ISV growth at 31 hpf and the presence of uninterrupted VV at 2 days post fertilization. Coinjection of *Danio rerio npnta* mRNA with *npnta*-MO2 partially rescued the ISV growth phenotype (**Figure S2, A and B**) and rescued the VV developmental phenotype in ~35% of the morphants (**Figure S2C**). Collectively, these data suggest that NPNT is required for VV and ISV morphogenesis.

Slower ISV growth and malformation of VV might be due to reduced EC proliferation. Hence, we determined whether *npnta* morphants exhibit related defects. For this purpose, control- and MO2-injected *Tg(etv2:EGFP)* embryos were incubated with 5-bromo-2'-deoxyuridine from 24 to 32 hpf and processed for incorporation at 32 hpf. Whereas in wild-type embryos, almost all ECs in the CVP were 5-bromo-2'-deoxyuridine positive; in *npnta* morphants, the number of 5-bromo-2'-deoxyuridine-positive ECs was slightly but significantly reduced by approximately 8% (**Figure 3A** and **3B**). Taken together, our data indicate that decreased ISV growth and VV malformation in *npnta* morphants are caused by hyposprouting of the AV, loss of directionality of the formed sprouts, and possibly also by reduced EC proliferation.

***Npnta* Mutants Phenocopy the Axial Vessel Phenotypes of *Npnta* Morphants**

Although in the past MOs have widely been used, concerns have been raised that it is difficult to

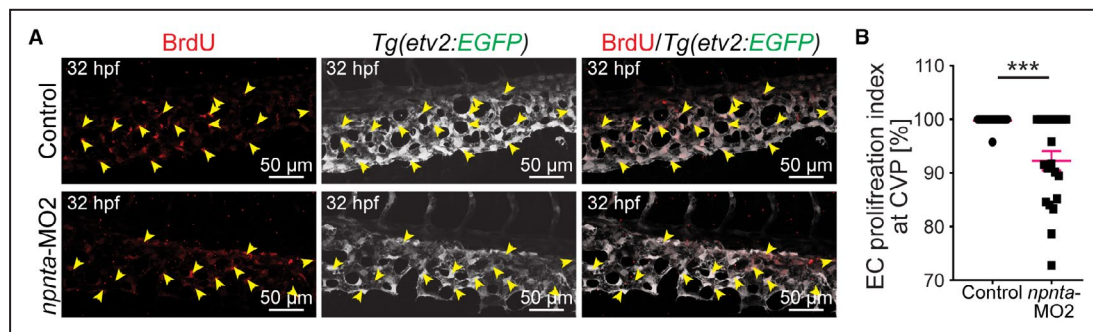


Figure 3. Decreased endothelial cell proliferation in the caudal vein plexus of *npnta* morphants.

A Maximum projections of confocal images of 32 hpf whole-mount embryos stained for 5-bromo-2'-deoxyuridine (red; marking proliferating cells) and EGFP (pseudo color; labeling ECs). Arrowheads indicate 5-bromo-2'-deoxyuridine⁺/EGFP⁺ cells. **B**, Quantitative analysis of EC proliferation at the caudal vein plexus. Graph representing the ratio of EGFP⁺/ethynyl-2'-deoxyuridine⁺ ECs relative to the total number of EGFP⁺ ECs at the CVP. A total of 24 control and 21 *npnta* morphants from 2 independent experiments were analyzed. The mean EC proliferative index for control embryos was considered as 100%. Statistical significance was determined by a 2-tailed Student's *t* test. Data are mean ± SEM. ****P* < 0.001. CVP indicates caudal vein plexus; EC, endothelial cell; EGFP, enhanced green fluorescent protein; hpf, hours post fertilization; and MO2 spliced blocking morpholino.

reliably discriminate between specific and nonspecific effects.⁵⁴ To confirm that *npnta* is required for AV sprouting and ISV growth, we generated a *npnta* mutant allele (*npnta*^{ari3}) that carries a frameshift-causing 10-nucleotide deletion on the fourth exon of the *npnta* locus (Figure S3). *npnta* mutants are fertile and viable. Because *npnta* morphants show decreased AV sprouting and ISV growth, we sought to compare the frequency of AV sprouting and the frequency of caudal ISVs reached DLAV in wild-type and *npnta* mutant embryos. Confocal microscopy of the post-cloaca caudal region of 28 hpf embryos from *Tg(etv2:EGFP)* transgenics revealed that in agreement with the *npnta* morphants, sprouting frequency of the AV was decreased by ~60% in *npnta* mutants compared with wild-type embryos at 28 hpf (Figure 4A and 4B). Moreover, at 30 hpf, whereas in wild-type embryos, ~60% of the 8 post-cloaca caudal ISVs reached the DLAV, in *npnta*^{-/-}, only ~10% of the 8 post-cloaca ISVs reached the DLAV (Figure 4C and 4D), suggesting slower ISV growth in *npnta* mutants compared with wild-type embryos. Overall, our data indicate that *npnta* mutants phenocopy the AV and ISV growth phenotype of the *npnta* morphants, confirming the necessity of *npnta* in axial vessel morphogenesis in zebrafish.

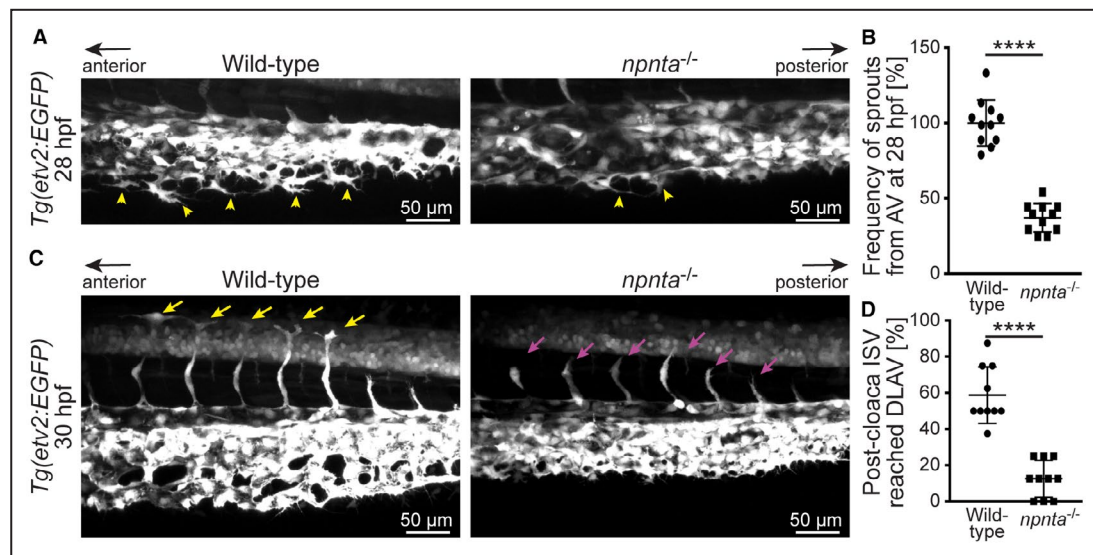
Nephronectin Interacts With Integrin α v β 3 Heterodimer

Integrins are positive key regulators of angiogenesis by interacting with their extracellular ligands.⁵⁵ NPNT has previously been shown to act as ligand of integrin α 8 β 1 regulating kidney morphogenesis and⁵⁶ migration of pericardial neural crest cells during corneal

development⁵⁷ and possibly lung development.⁵⁸ Yet, integrin α 8 β 1 has so far not been associated with vessel formation. Moreover, in situ hybridization revealed that *itga8* is not expressed in the CVP during 20 to 32 hpf, whereas *itga8* expression was detected in the tail bud at 20 to 24 hpf and in the posterior somites at 32 hpf (Figure S4). This indicates that *npnta* does not control CVP formation by interacting with *Itga8*. Therefore, we tested whether *itgav*, an integrin subunit known to be associated with angiogenesis,⁵⁹ is coexpressed with *npnta*. Sagittal and transverse sections through the whole-mount in situ hybridized embryo indicate that *itgav* is co-expressed with *npnta* in the CVP forming region and posterior somites at 30 hpf (Figure 5A). For functional activation, the α v subunit forms heterodimers with β 1, β 3, β 5, β 6, or β 8 subunit.⁵¹ Here we found that *itgb3.1*, the zebrafish orthologue of mammalian *ITGB3*, is also expressed at the CVP and in the ventral region of the posterior somites at 30 hpf (Figure 5B). To determine if NPNT and ITGAV can interact, Flag-tagged human NPNT, ITGAV, and ITGB3 subunits were ectopically expressed in HEK293T cells. Coimmunoprecipitation experiments showed that the pull-down of FLAG-tagged NPNT by anti-FLAG antibody readily coprecipitated ITGAV and ITGB3 (Figure 5C). These data indicate that NPNT is a ligand of integrin α v β 3 and this interaction might control CVP morphogenesis.

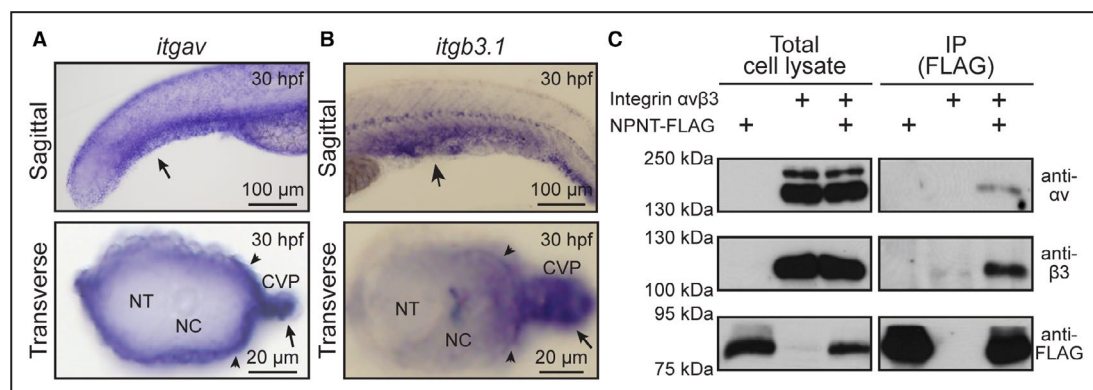
Itgav Knockdown Phenocopies the Axial Vessel Phenotypes in *Npnta* Morphants and Mutants

To substantiate the hypothesis that *Npnta* regulates axial vessel morphogenesis through integrin α v β 3 in



zebrafish, we tested whether morpholino-mediated knockdown of *itgav* will result in similar phenotypes as observed in *npnta* morphants or mutants. For this purpose, single cell-stage embryos were injected with a previously established translation-blocking morpholino targeting *itgav*.⁵¹ Similar to *npnta* morphants and *npnta*

mutants, *itgav* knockdown resulted in hyposprouting of the posterior AV at 28 hpf as well as in abnormal CVP and VV morphogenesis (Figure 6A and 6B). In addition, at 31 hpf, whereas ~80% of the 8 post-cloaca caudal ISVs reached the DLAV in control embryos, in *itgav*^{-/-}, most of these ISVs failed to reach the DLAV (Figure 6C



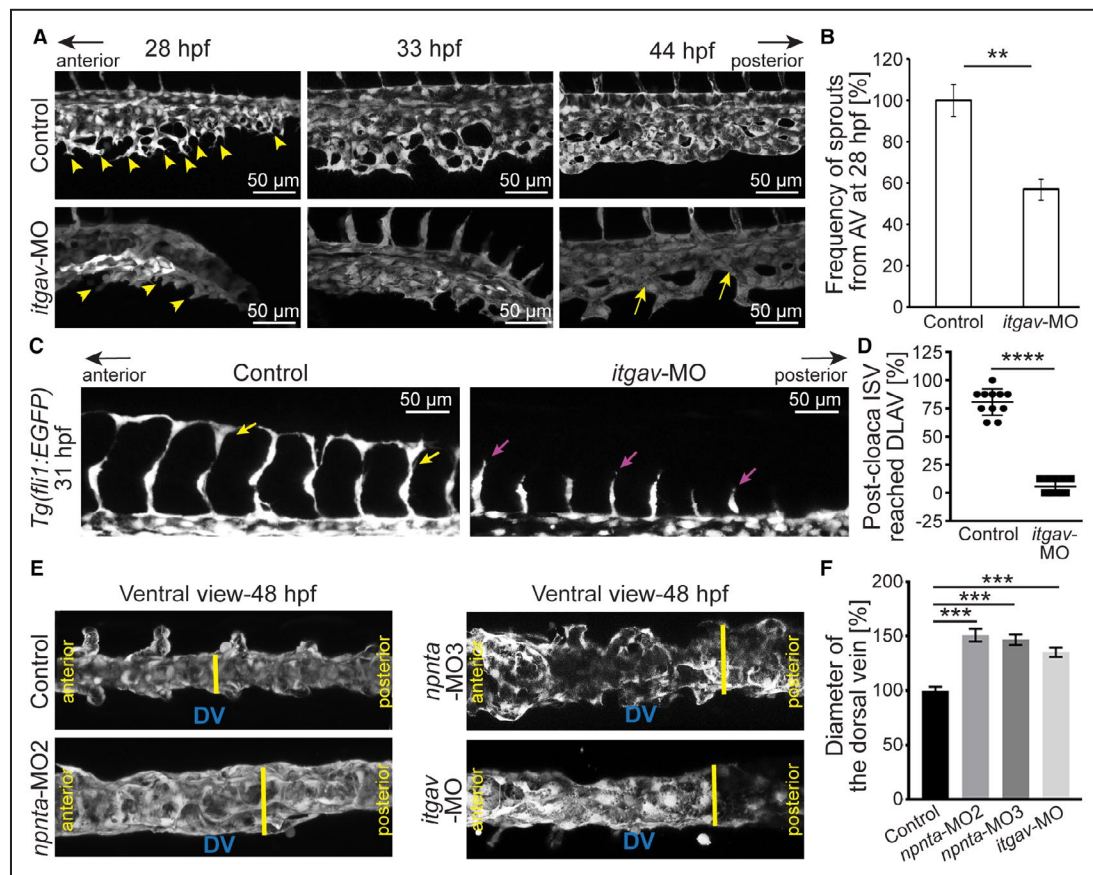


Figure 6. *itgav* knockdown phenocopies *npnta* morphants and mutants.

A, Lateral views of the maximum intensity projections of confocal images of caudal vein plexus from control- and *itgav* morpholino-injected *Tg(fli1:EGFP)* zebrafish embryos. Arrowheads indicate angiogenic sprouts from the posterior axial vein and arrows point to discontinuation of ventral vein. **B**, Quantification of the frequency of angiogenic sprouts at CVP at 28 hpf (n=6 embryos for each group). The mean frequency of angiogenic sprouts in the control embryos was considered 100%. **C**, Maximum intensity projections of the confocal images of the caudal region show ISVs from the dorsal artery. **D**, Quantification of 8 post-cloaca ISVs from each animal reached the dorsal lateral anastomotic vessel at 31 hpf (n=12 embryos for each group). **E**, Ventral views of 3-dimensional projections of confocal images of the DV from control-, MO2-, MO3-, or *itgav* morpholino-injected *Tg(fli1:EGFP)* zebrafish embryos. Yellow lines: the maximum thickness of the DV from the ventral view. **F**, Quantification of the thickness of the DV at 48 hpf from ventral view (n=6 embryos for each group). The mean value of the control was considered 100% in each case. Statistical significance in **B** and **D** was determined by a 2-tailed Student's *t* test and in **F** by 1-way ANOVA followed by a post hoc test. Data are mean±SEM. ***P*≤0.01; ****P*≤0.001. AV indicates axial vein; CVP, caudal vein plexus; DLAV, dorsal lateral anastomotic vessel; DV, dorsal vein; hpf, hours post fertilization; ISV, intersegmental vessel; and MO2,3 spliced blocking morpholino.

and 6D), suggesting slower ISV growth, which is similar to the age-matched *npnta* morphants and mutants. Ventral view of the DV at 48 hpf revealed that the DV of both *npnta* and *itgav* morphants are broader than control embryos at 48 hpf (Figure 6E and 6F), suggesting that ECs, which failed to migrate ventrally, might have remained at the DV.

Our preceding in vitro analysis showed that NPNT interacts with ITGAV. Thus, we explored whether a combined subcritical knockdown of *npnta* and *itgav* phenocopy the axial vessel morphogenesis phenotype of the *npnta* or *itgav* morphants. A 50% dose of MO2

(1.2 ng/embryo) or *itgav*-MO (0.5 ng/embryo) showed ~10% inhibition on AV sprouting and ~15% inhibition on ISV growth in comparison to the control embryos (Figure S5). However, a combinatorial 50% dose of MO2 and *itgav*-MO injection resulted in ~70% decreased AV sprouting and ~90% decreased ISV growth in comparison to the control embryos (Figure S5), which is comparable to the axial vessel phenotype in full-dose *npnta* morphants (2.4 ng/embryo; Figure 2) or *itgav* morphants (1 ng/embryo; Figure 6). These data support that *Npnta* regulates AV sprouting and ISV formation via interacting with Itgav. Overall, our results

indicate that *Npnta* acts as an Itgav ligand controlling ISV growth and EC sprouting from the AV to form VV.

Npnta Is Required for Blood Vessel Maturation During Adult Zebrafish Fin Regeneration

During regeneration of the amputated caudal fin in adult zebrafish, after the initial healing of the wound surface, the distal tip of the existing vessels starts to sprout and extend distally.⁶⁰ Over time, these thin vessels get connected to each other and form a vascular plexus. In the next step, the unstructured weak vessels prune back and form the matured vessels at the proximal side, leading to the development of a more ordered vasculature.⁶⁰ Thus, we used the zebrafish caudal fin regeneration model to explore the role of *Npnta* during early angiogenesis (plexus development) and maturation (formation of the arteries and veins from the vessel plexus) in adults. The study revealed that the degree of fin regeneration and the average length of newly formed vessel plexus in the regenerated fin was indistinguishable between wild-type and *npnta* mutant zebrafish at 5 days post amputation (Figure 7A and 7B). In contrast, the length of the matured vessel at the proximal end of the regenerated vessels in the regenerating caudal fins was significantly shorter in *npnta* mutants compared with wild-type zebrafish at 5 days post amputation (Figure 7A and 7C). Therefore, we conclude

that *Npnta* is required for blood vessel formation or maturation during adult tissue regeneration.

Nephronectin Promotes Mammalian Angiogenesis and Vessel Maturation

The zebrafish is an excellent vertebrate model with high homology to humans (47% of human genes have a single zebrafish ortholog, whereas ~24% of human genes have more than 1 zebrafish ortholog).^{61,62} Yet, it is important to validate findings in zebrafish in a mammalian system. Therefore, we have assessed the role of mr-NPNT in EC proliferation, migration, and stability of capillary-like EC tubes using HUVECs. First, the effect of mr-NPNT on EC proliferation was explored by ethynyl-2'-deoxyuridine incorporation assay. Quantification did not show any significant effect on ethynyl-2'-deoxyuridine incorporation by HUVECs in mr-NPNT-coated plates compared with gelatin-coated plates in the absence or presence of serum (Figure S6). Then, scratch assays were performed on HUVECs at a confluency of ~95%, seeded on mr-NPNT- or gelatin-coated tissue culture plates. Six-hour post-scratch cells on gelatin-coated plates covered $32.16 \pm 2.47\%$ of the scratched area. In contrast, HUVECs on NPNT-coated plates covered $53.76 \pm 3.8\%$ of the scratch area ($n=3$, $P \leq 0.05$; Figure 8A and 8B). These data suggest that NPNT promotes mammalian EC migration. Next, we determined the effect of NPNT on tube formation by assessing capillary-like tube formation by HUVECs

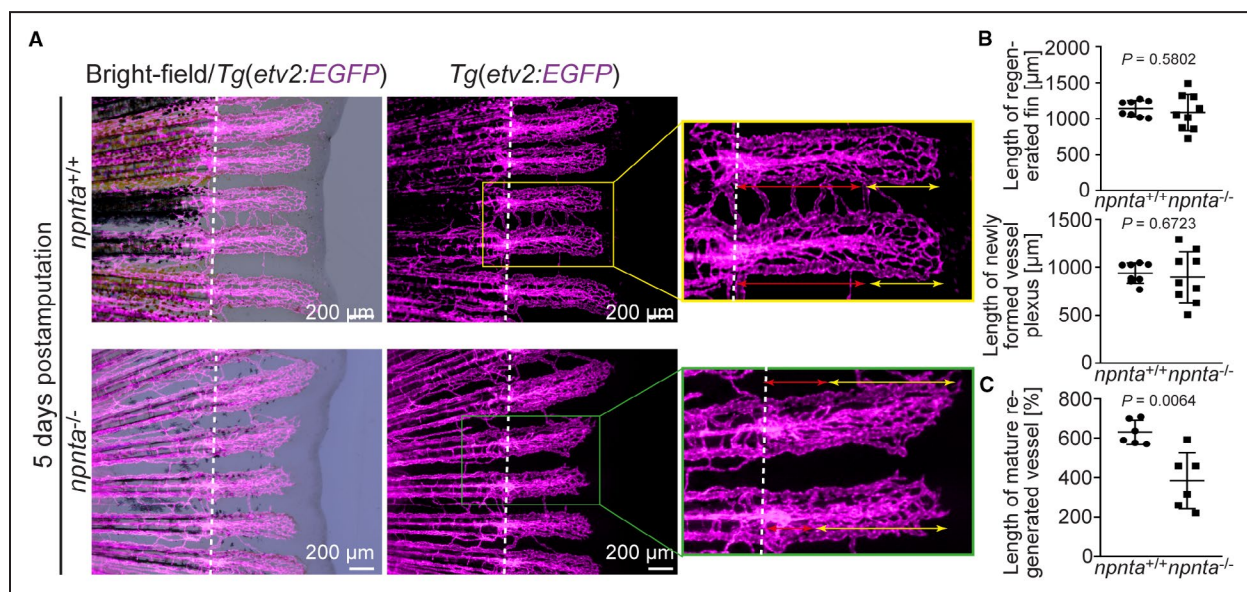


Figure 7. Adult *npnta* mutants exhibit decreased vessel pruning during caudal fin regeneration.

A, Representative overlays of bright-field and epifluorescence images as well as epifluorescence images of individual caudal fins of a wild-type and *npnta* mutant in a *Tg(etv2:EGFP)* background at 5 days post amputation revealing decreased vessel maturation (magenta; endothelial cell membrane) during caudal fin regeneration. Double-sided yellow arrows: length of neovascular plexus. Double-sided red arrows: length of matured neovessels. Scale bars: 200 μm. **B**, Quantitative analysis of the length of regenerated fins and the length (μm) of regenerated blood vessels. **C**, Quantification of the length of the matured blood vessels at the proximal ends of the regenerated fins. Statistical significance was determined by a 2-tailed Student's *t* test. Data are mean ± SEM. ns: *P* > 0.05, and ***P* ≤ 0.01.

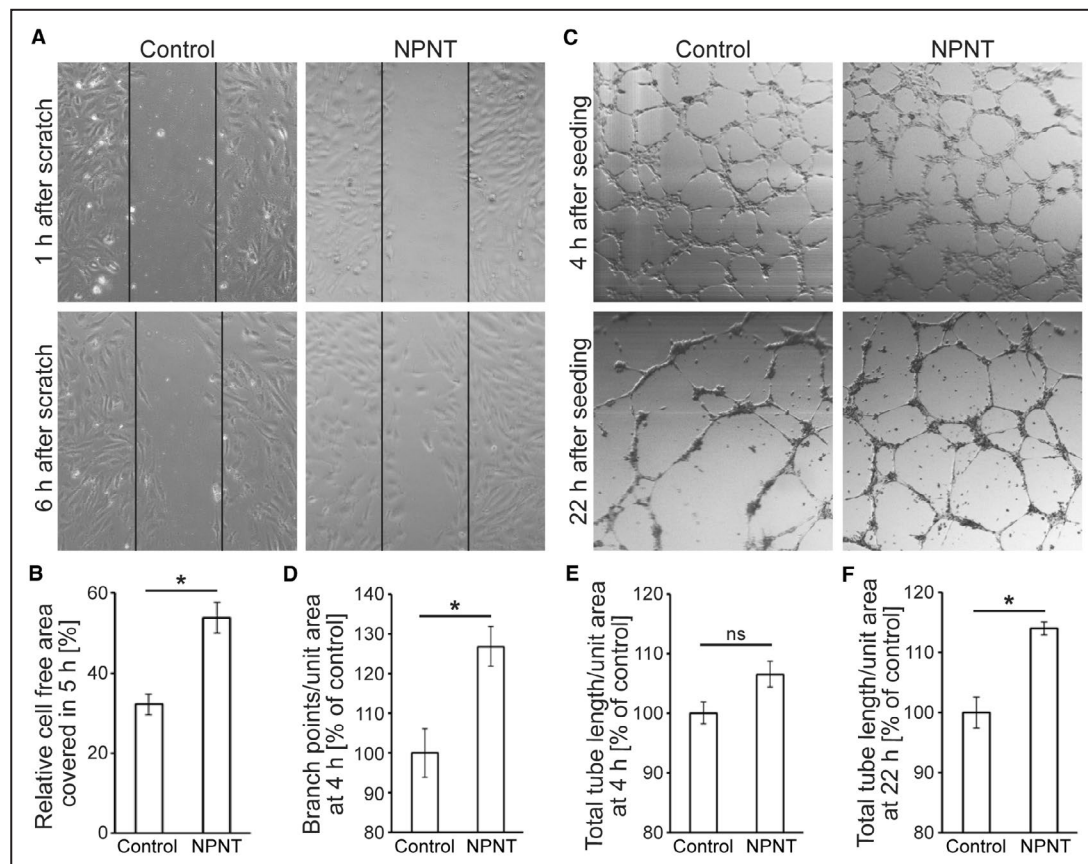


Figure 8. Nephronectin promotes HUVEC migration, tube formation, and stabilization *in vitro*.

A, Cell migration assay: representative brightfield images of wound assays 1 and 6 hours after scratching. Cells were cultured on gelatin- (control) or mr-NPNT-coated 24-well cell culture plates. **B**, Quantitative analysis of cell migration (n=4). The mean value of the control was considered 100% in each case. **C**, Tube formation assay: representative brightfield images of HUVECs cultured on Matrigel with BSA (10 μ g/mL, control) or mr-NPNT (10 μ g/mL) at 4 and 22 hours after seeding. **D–F**, Quantitative analysis of tube branching (**D**), and tube stability (**E**, **F**) (n=4). Mean value of the control was considered 100% in each case. Statistical significance was determined by a 2-tailed Student's *t* test. Data are mean \pm SEM. ns: $P>0.05$. * $P\leq 0.05$. HUVEC indicates human umbilical vascular endothelial cell; and mr-NPNT, recombinant mouse nephronectin.

on Matrigel. HUVECs seeded on the surface of casted Matrigel exhibited a peak in tube formation between 3 to 12 hours post seeding.⁶³ Here, we determined branch point frequency per unit area at 4 hours post seeding, comparing Matrigel containing BSA (control) or mr-NPNT. Quantitative analysis revealed that HUVEC tubular networks on mr-NPNT-containing Matrigel had $26.81\pm 5.09\%$ more branch points than on BSA-containing control Matrigel (Figure 8C and 8D). Although analysis of the total tube length per unit area showed a trend toward a longer total tube length in mr-NPNT-containing than BSA-containing control Matrigel, the difference was not significant (Figure 8C and 8E; n=4, $P>0.05$). Interestingly, total tube length per unit area at 22 hours post seeding, a time when HUVEC-based tubes on Matrigel usually deteriorate,⁶³ was significantly higher (by 14%) in mr-NPNT-containing Matrigel in comparison to the BSA control (n=4, $P<0.05$; Figure 8C and 8F), suggesting NPNT

promotes vessel stability *in vitro*. Collectively, these data suggest that NPNT can directly promote tube formation and increase tube stability in HUVECs, thus, in mammalian angiogenesis.

To further substantiate this conclusion, we determined the effect of mr-NPNT on mammalian angiogenesis in an *ex vivo* aortic ring assay. Approximately 1 mm long rings of murine thoracic aortae were embedded in a type I collagen (collagen-I) matrix. After 7 days of culture, periaortic vascular sprouting distance was increased by approximately 48% in presence of mr-NPNT compared with the untreated control (Figure 9A and 9B). VEGF alone, used as a positive control, resulted in pronounced capillary sprout formation extending large distances as expected. This effect was not significantly enhanced by the simultaneous application of VEGF and mr-NPNT (Figure 9A and 9B). However, the presence of mr-NPNT in aortic rings treated with VEGF enhanced periaortic vascular

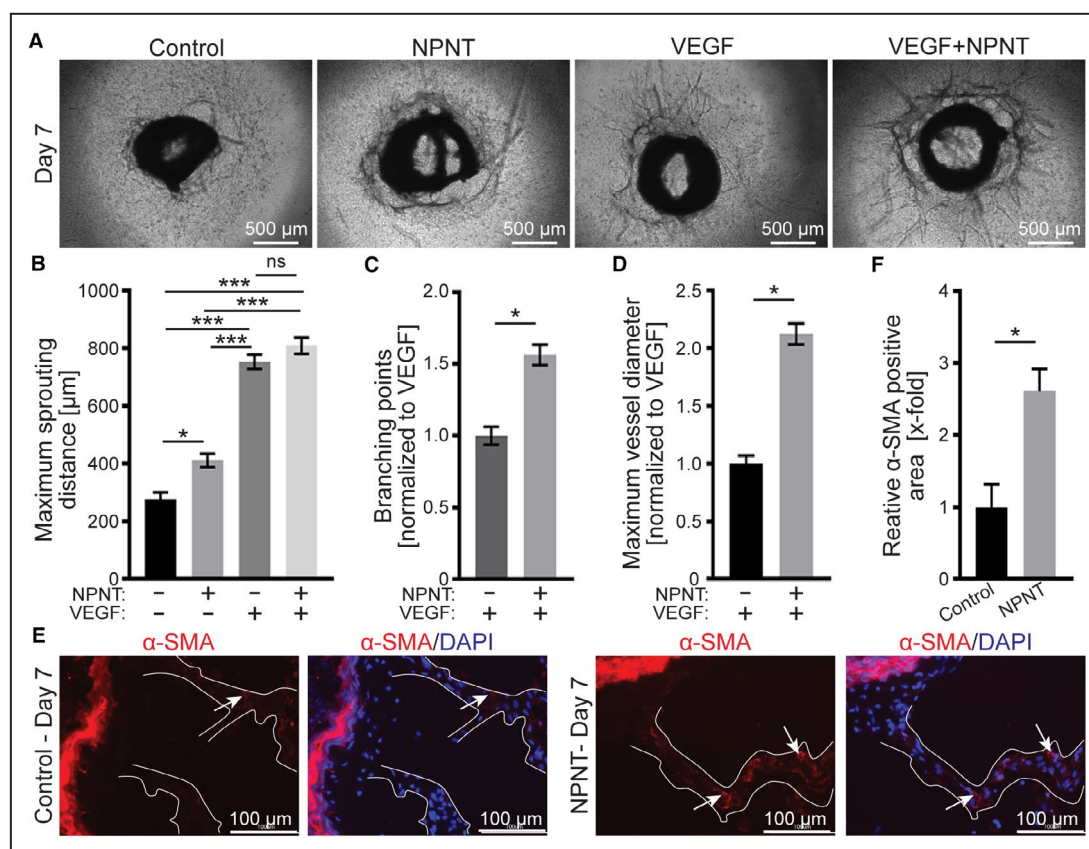


Figure 9. Nephronectin promotes intercapillary network formation and smooth muscle cell recruitment. **A**, Phase-contrast images of aortic rings at 7 days in culture. Aortic rings were embedded in collagen-I solution and cultured in supplemented Opti-MEM culture medium with or without VEGF or/and recombinant mouse NPNT in 96-well cell culture plates. **B–D**, Quantitative analysis of maximum distance covered by angiogenic sprouts (n=7) (**B**), periaortic vascular capillary branch points density (n=4) (**C**), and the maximum diameter of the periaortic vessels (n=9) (**D**). **E** and **F**, Representative examples of the appearance of pericytes/smooth muscle cells (α-smooth muscle Actin-positive, arrows) surrounding vascular sprouts (**E**) and quantitative analysis (**F**). Statistical significance in (**B**) was determined by 1-way ANOVA followed by a pos hoc test and in (**C–F**) by a 2-tailed Student's *t* test. Data are mean±SEM. ns: *P*≥0.05; **P*≤0.05; ****P*≤0.001. α-SMA indicates α-smooth muscle actin; DAPI, 4',6-diamidino-2-phenylindole; NPNT, nephronectin; and VEGF, vascular endothelial growth factor.

capillary interconnectivity by approximately 56% as indicated by vascular branching point quantification (Figure 9A and 9C). Interestingly, capillary vessel diameter was also increased by approximately 112% when VEGF and mr-NPNT were applied simultaneously compared with VEGF alone (Figure 9A and 9D).

As our tube formation assay suggested that mr-NPNT promotes tube stability, we asked whether mr-NPNT can stimulate vascular maturation in an aortic ring assay. Appearance of pericytes/smooth muscle cells surrounding the vascular sprouts is one of the hallmarks of vessel maturation as they protect neo-vasculature from regression.⁶⁴ Our data indicate that the presence of mr-NPNT in aortic ring culture enhanced recruitment of smooth muscle alpha-actin expressing cells surrounding the vascular sprouts from the aortic ring (Figure 9E and 9F), suggesting NPNT promotes vessel maturation under ex vivo conditions.

Collectively, our data support that NPNT enhances mammalian vascular growth, network formation, and vascular maturation by recruiting α-smooth muscle actin positive pericytes or smooth muscle cells.

Nephronectin Enhances Tube Formation in Hydrogels

Our in vivo studies on zebrafish embryos and ex vivo aortic ring assay identified NPNT as a proangiogenic molecule, which promotes vessel growth, networking, maturation, and stability of vessels. Thus, we intended to evaluate whether NPNT can be a beneficial ECM molecule for tissue engineering applications. For this purpose, HUVECs were resuspended in a pregel solution of collagen-I (control) or collagen-I containing 10 μg/mL mr-NPNT to explore the influence of NPNT on tube formation and stability in 3D. The constructs

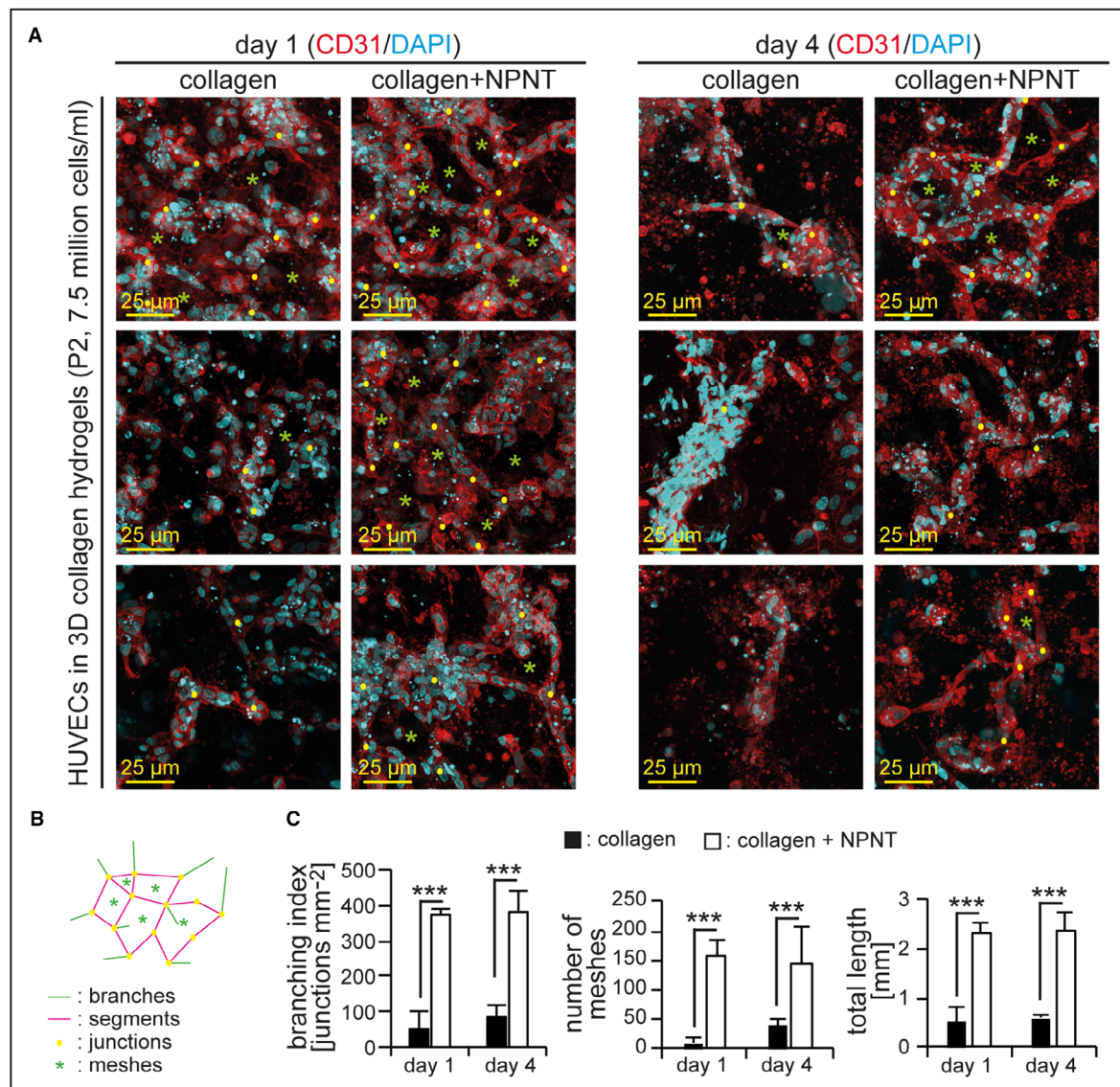


Figure 10. mr-NPNT enhances vessel formation in hydrogels.

A, Examples of projections of confocal images of HUVECs (passage number 2, P2) cultured in collagen-I-based hydrogels stained for endothelial specific marker CD31 and DNA by 4',6-diamidino-2-phenylindole. Yellow dots: examples of junctions. Green asterisks: examples of meshes. **B**, Schematic of a vascular network indicating measured parameters. **C**, Quantitative analysis of **(A)** ($n=3$) regarding vasculature complexity based on branching index, number of meshes, and total length (segments + branches). Statistical significance was determined by a 2-tailed Student's t test. Data are mean \pm SEM. *** $P\leq 0.001$. DAPI indicates 4',6-diamidino-2-phenylindole; HUVEC, human umbilical vascular endothelial cell; mr-NPNT, recombinant mouse nephronectin.

were incubated at 37 °C to gel. After 24 hours (1 day) or 4 days, constructs were fixed, and tube formation was evaluated based on immunostained images (ECs: CD31. 4',6-diamidino-2-phenylindole: DNA/nuclei). Our data show that after 1 day, cells in collagen-I-based hydrogels spread and start to connect and potentially initiate tubular network formation (Figure 10A). The presence of mr-NPNT enhanced this process resulting in more complex tubular networks (Figure 10A). These more complex networks in the presence of mr-NPNT

were maintained on day 4 and remained more complex compared with tubular networks in collagen-I-based hydrogels in the absence of mr-NPNT, based on a higher branching index and number of meshes, quantitated with the Angiogenesis Analyzer plugin of NIH Image J software⁶⁵ (Figure 10B and 10C). Although HUVECs could form tubular structures in collagen without mr-NPNT, it was sporadic and the formed structures were relatively less complex, which is similar to our findings based on aortic ring assay (Figure 9A

and 9D). These data suggest that NPNT could be used to engineer better vascularized tissues.

DISCUSSION

Whether NPNT regulates vascularization in vivo, how it cooperates with major regulators of vascularization and its role in vessel stability and maturation were unknown. Here, we used loss of function approaches and protein–protein interaction assays to show that NPNT is required for physiological angiogenesis and acts as a ligand of the integrin $\alpha\beta3$ heterodimer. Notably, integrin $\alpha\beta3$ is known to be required for EC proliferation⁶⁶ as well as vascular drift, structural rearrangements (eg, vascular fusion), individual cell migration along existing endothelial structures, and cell process extension into avascular areas, resulting in new links within a vascular plexus.⁶⁷ Furthermore, many EGF-like protein family members such as EGFL7 (EGF-like domain-containing protein 7) promote endothelial cell migration and angiogenesis, whereby ectopic EGFL7 has also shown to bind to the integrin $\alpha\beta3$ heterodimer to enhance vessel formation.^{68,69} These published data support our findings and conclusion that NPNT regulates vascular morphogenesis by direct cellular interaction via integrin $\alpha\beta3$ binding.

A major bottleneck in tissue engineering is the need of vascularization in order to produce thick constructs, which can be implanted to stabilize or enhance function of injured or lost tissues/organs. Although thick constructs can be engineered and maintained in vitro by providing “channels” that allow to provide oxygen and nutrients via medium, their implantation in vivo will result at least in partial deterioration until the transplant will be vascularized by the host organism as the “channels” cannot be connected to the host vasculature without a proper functional endothelialization. In addition, such a channel structure might impair function of the construct. Previously, it has been reported that mr-NPNT enhances migration and tube formation of simian virus 40-transformed mouse microvascular endothelial cells

via ERK1/2 (extracellular signal-regulated kinase 1/2) signaling and HUVECs via EGF receptor/JAK2 (Janus kinase)/STAT3 (signal transducer and activator of transcription) signaling. In addition, mr-NPNT induced vessel outgrowth from metatarsals and adenoviral overexpression of NPNT in mouse hearts 4 weeks before an experimental myocardial infarction resulted in a slight improvement in heart function and increased angiogenesis in the infarct border zone.^{45,46} Our data confirm that ectopic NPNT promotes EC migration, tube formation, and vessel outgrowth from existing vessels. Importantly, our data show a synergistic effect between VEGF and NPNT regarding vascular branching, capillary vessel diameter, and recruitment of smooth muscle alpha-actin expressing cells. This is important, as VEGF is extremely potent in inducing vessel sprouting, but it is not sufficient to induce vessel maturation. VEGF-induced vessels remain leaky and immature.⁴⁸ the effect on recruitment of smooth muscle alpha-actin expressing cells is especially of interest here. Notably, integrin $\alpha8\beta1$, the receptor of NPNT,³⁶ is most abundantly expressed in vascular smooth muscle cells.^{70–72} In the future, it will be important to study in detail how NPNT can be used to engineer vascularized tissue, like heart tissue, for example in the combination with VEGF and other proangiogenic factors.

CONCLUSION

We conclude that NPNT is a proangiogenic factor that is required for vessel formation during embryonic development and can be used to improve vascularization of engineered tissues. One important mechanism underlying the function of NPNT is its interaction with the integrin $\alpha\beta3$ receptor (Figure 11). Several lines of evidence support these conclusions. First, *npnta* knockdown as well as *npnta* loss-of-function results in diminished AV sprouting, ISV growth, and impaired VV morphogenesis. Second, *itgav* and *itgb3.1* are co-expressed with *npnta* in the CVP and surrounding tissue during CVP morphogenesis. Third, *itgav* morphants phenocopy

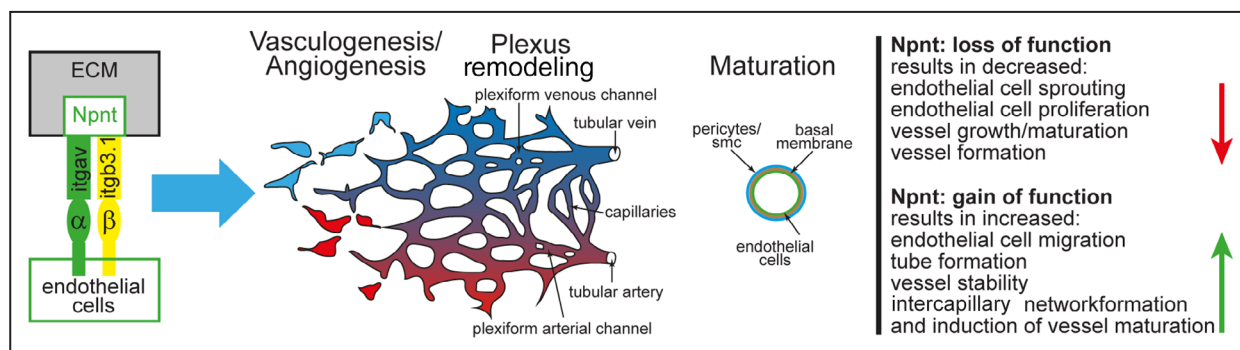


Figure 11. Summary of the role of nephronectin in angiogenesis.

ECM indicates extracellular matrix; and Smc, smooth muscle cells.

npnta morphants and mutants. Fourth, NPNT interacts with integrin $\alpha\beta3$. Moreover, NPNT promoted mammalian angiogenesis and vessel stability and enhanced VEGF-induced periaortic vascular capillary interconnectivity and capillary vessel diameter. Finally, NPNT showed proangiogenic properties in collagen-I-based hydrogels.

Collectively, our in vivo and in vitro data indicate that NPNT is a proangiogenic factor suitable to enhance vascularization strategies in tissue engineering.

ARTICLE INFORMATION

Received August 8, 2024; accepted December 5, 2024.

Affiliations

Department of Developmental Biology, Agharkar Research Institute, Pune, India (C.P., A.R., G.W.); Institute of Anatomy and Cell Biology II, Julius-Maximilians-University, Würzburg, Germany (F.K., S.E.); Experimental Renal and Cardiovascular Research, Department of Nephropathology, Institute of Pathology and Department of Cardiology, Friedrich-Alexander-Universität Erlangen-Nürnberg (FAU), Erlangen, Germany (K.R., F.B.E.); Institute of Cell Biology and Neuroscience, Johann Wolfgang Goethe University Frankfurt am Main, Frankfurt am Main, Germany (F.C., A.A.-P.); Department of Biochemistry and Molecular Biology, Monash Biomedicine Discovery Institute, Monash University, Clayton, Australia (I.N.); Institute of Anatomy, Medical Faculty Carl Gustav Carus, Technische Universität Dresden School of Medicine, Dresden, Germany (M.H.H.S.).

Acknowledgments

We thank the technical staff for excellent fish care at ARI, Pune, and MPI, Bad Nauheim, Germany. Author contributions: Conceptualization: Chinmoy Patra, Felix B. Engel; Formal analysis: Chinmoy Patra, Ganesh Wagh, Florian Cop, Kaveh Roshanbinfar; Investigation: Chinmoy Patra, Amey Rayrikar, Ganesh Wagh, Florian Kleefeldt, Kaveh Roshanbinfar, Florian Cop, Iva Nikolic; Visualization: Chinmoy Patra, Kaveh Roshanbinfar, Süleyman Ergün, Felix B. Engel; Data curation: Chinmoy Patra, Felix B. Engel; Supervision: Chinmoy Patra, Mirko H. H. Schmidt, Amparo Acker-Palmer, Süleyman Ergün, Felix B. Engel; Writing—original draft: Chinmoy Patra, Felix B. Engel; Writing—review and editing: Amey Rayrikar, Ganesh Wagh, Florian Kleefeldt, Kaveh Roshanbinfar, Florian Cop, Iva Nikolic, Mirko H. H. Schmidt, Amparo Acker-Palmer, Süleyman Ergün, Felix B. Engel; Project administration: Felix B. Engel, Chinmoy Patra; Funding acquisition: Chinmoy Patra, Süleyman Ergün, Felix B. Engel.

Sources of Funding

This work was supported by the Max-Planck-partner group Award, Max-Planck-Society, Germany and Department of Science and Technology, India (Chinmoy Patra).

Department of Biotechnology/Wellcome Trust India Alliance Intermediate Fellowship (Ref# IA/11/18/2/504016; Chinmoy Patra), Deutsche Forschungsgemeinschaft, Projektnummer 326998 133 – TRR 225/C01 (Felix B. Engel), Deutsche Forschungsgemeinschaft, Projektnummer 326998 133 – seed fund (Kaveh Roshanbinfar), Deutsche Forschungsgemeinschaft, Projektnummer 326998 133 – TRR 225/B04 (Süleyman Ergün), Deutsche Forschungsgemeinschaft, INST 410/91-1 FUGG (Felix B. Engel), Deutsche Forschungsgemeinschaft, SFB834, SFB1531 (Amparo Acker-Palmer), Universitätsklinikum Erlangen ELAN IZKF (Interdisciplinary Center for Clinical Research), grant number P093/ Aktenzeichen: 21–05-20-1-Roshanbinfar (Kaveh Roshanbinfar), Deutsche Forschungsgemeinschaft, SFB688/TPA19 (Süleyman Ergün), Deutsche Herzzstiftung e.V., Alexander von Humboldt Foundation award Sofja Kovalevskaja Award (Felix B. Engel).

Disclosures

None.

Supplemental Material

Figures S1–S6.

REFERENCES

- Blanco R, Gerhardt H. VEGF and notch in tip and stalk cell selection. *Cold Spring Harb Perspect Med*. 2013;3:a006569. doi: [10.1101/cshperspect.a006569](https://doi.org/10.1101/cshperspect.a006569)
- Isogai S, Lawson ND, Torrealday S, Horiguchi M, Weinstein BM. Angiogenic network formation in the developing vertebrate trunk. *Development*. 2003;130:5281–5290. doi: [10.1242/dev.00733](https://doi.org/10.1242/dev.00733)
- Gerhardt H, Golding M, Fruttiger M, Ruhrberg C, Lundkvist A, Abramsson A, Jeltsch M, Mitchell C, Alitalo K, Shima D, et al. VEGF guides angiogenic sprouting utilizing endothelial tip cell filopodia. *J Cell Biol*. 2003;161:1163–1177. doi: [10.1083/jcb.200302047](https://doi.org/10.1083/jcb.200302047)
- Tammela T, Zarkada G, Wallgard E, Murtomaki A, Suchting S, Wirzenius M, Waltari M, Hellstrom M, Schomber T, Peltonen R, et al. Blocking VEGFR-3 suppresses angiogenic sprouting and vascular network formation. *Nature*. 2008;454:656–660. doi: [10.1038/nature07083](https://doi.org/10.1038/nature07083)
- Potente M, Gerhardt H, Carmeliet P. Basic and therapeutic aspects of angiogenesis. *Cell*. 2011;146:873–887. doi: [10.1016/j.cell.2011.08.039](https://doi.org/10.1016/j.cell.2011.08.039)
- Hellstrom M, Phng LK, Hofmann JJ, Wallgard E, Coultas L, Lindblom P, Alva J, Nilsson AK, Karlsson L, Galiano N, et al. Dll4 signalling through Notch1 regulates formation of tip cells during angiogenesis. *Nature*. 2007;445:776–780. doi: [10.1038/nature05571](https://doi.org/10.1038/nature05571)
- Leslie JD, Ariza-McNaughton L, Bermange AL, McAdow R, Johnson SL, Lewis J. Endothelial signalling by the notch ligand Delta-like 4 restricts angiogenesis. *Development*. 2007;134:839–844. doi: [10.1242/dev.003244](https://doi.org/10.1242/dev.003244)
- Sainson RC, Aoto J, Nakatsu MN, Holderfield M, Conn E, Koller E, Hughes CC. Cell-autonomous notch signaling regulates endothelial cell branching and proliferation during vascular tubulogenesis. *FASEB J*. 2005;19:1027–1029. doi: [10.1096/fj.04-3172fje](https://doi.org/10.1096/fj.04-3172fje)
- Xu Q, Wang Y, Dabdoub A, Smallwood PM, Williams J, Woods C, Kelley MW, Jiang L, Tasman W, Zhang K, et al. Vascular development in the retina and inner ear: control by norrin and Frizzled-4, a high-affinity ligand-receptor pair. *Cell*. 2004;116:883–895. doi: [10.1016/S0092-8674\(04\)00216-8](https://doi.org/10.1016/S0092-8674(04)00216-8)
- Wiley DM, Kim JD, Hao J, Hong CC, Baatch VL, Jin SW. Distinct signalling pathways regulate sprouting angiogenesis from the dorsal aorta and the axial vein. *Nat Cell Biol*. 2011;13:686–692. doi: [10.1038/ncb2232](https://doi.org/10.1038/ncb2232)
- Navankasattusas S, Whitehead KJ, Suli A, Sorensen LK, Lim AH, Zhao J, Park KW, Wythe JD, Thomas KR, Chien CB, et al. The netrin receptor UNC5B promotes angiogenesis in specific vascular beds. *Development*. 2008;135:659–667. doi: [10.1242/dev.013623](https://doi.org/10.1242/dev.013623)
- Sakurai A, Doci CL, Gutkind JS. Semaphorin signaling in angiogenesis, lymphangiogenesis and cancer. *Cell Res*. 2012;22:23–32. doi: [10.1038/cr.2011.198](https://doi.org/10.1038/cr.2011.198)
- Adams RH, Diella F, Hennig S, Helmbacher F, Deutsch U, Klein R. The cytoplasmic domain of the ligand ephrinB2 is required for vascular morphogenesis but not cranial neural crest migration. *Cell*. 2001;104:57–69. doi: [10.1016/S0092-8674\(01\)00191-X](https://doi.org/10.1016/S0092-8674(01)00191-X)
- Adams RH, Wilkinson GA, Weiss C, Diella F, Gale NW, Deutsch U, Risau W, Klein R. Roles of ephrinB ligands and EphB receptors in cardiovascular development: demarcation of arterial/venous domains, vascular morphogenesis, and sprouting angiogenesis. *Genes Dev*. 1999;13:295–306. doi: [10.1101/gad.13.3.295](https://doi.org/10.1101/gad.13.3.295)
- Hynes RO. Integrins: bidirectional, allosteric signaling machines. *Cell*. 2002;110:673–687. doi: [10.1016/S0092-8674\(02\)00971-6](https://doi.org/10.1016/S0092-8674(02)00971-6)
- Wang X, Harris RE, Bayston LJ, Ashe HL. Type IV collagens regulate BMP signalling in drosophila. *Nature*. 2008;455:72–77. doi: [10.1038/nature07214](https://doi.org/10.1038/nature07214)
- Suehiro K, Gailit J, Plow EF. Fibrinogen is a ligand for integrin $\alpha5\beta1$ on endothelial cells. *J Biol Chem*. 1997;272:5360–5366. doi: [10.1074/jbc.272.8.5360](https://doi.org/10.1074/jbc.272.8.5360)
- Albig AR, Becenti DJ, Roy TG, Schiemann WP. Transcriptome analysis of endothelial cell gene expression induced by growth on matrigel matrices: identification and characterization of MAGP-2 and lumican as novel regulators of angiogenesis. *Angiogenesis*. 2007;10:197–216. doi: [10.1007/s10456-007-9075-z](https://doi.org/10.1007/s10456-007-9075-z)
- Albig AR, Becenti DJ, Roy TG, Schiemann WP. Microfibril-associate glycoprotein-2 (MAGP-2) promotes angiogenic cell sprouting by blocking notch signaling in endothelial cells. *Microvasc Res*. 2008;76:7–14. doi: [10.1016/j.mvr.2008.01.001](https://doi.org/10.1016/j.mvr.2008.01.001)
- Miyamoto A, Lau R, Hein PW, Shipley JM, Weinmaster G. Microfibrillar proteins MAGP-1 and MAGP-2 induce Notch1 extracellular domain

- dissociation and receptor activation. *J Biol Chem*. 2006;281:10089–10097. doi: [10.1074/jbc.M600298200](#)
21. Pufe T, Petersen WJ, Miosge N, Goldring MB, Mentlein R, Varoga DJ, Tillmann BN. Endostatin/collagen XVIII—an inhibitor of angiogenesis—is expressed in cartilage and fibrocartilage. *Matrix Biol*. 2004;23:267–276. doi: [10.1016/j.matbio.2004.06.003](#)
 22. Lee NV, Sato M, Annis DS, Loo JA, Wu L, Mosher DF, Iruela-Arispe ML. ADAMTS1 mediates the release of antiangiogenic polypeptides from TSP1 and 2. *EMBO J*. 2006;25:5270–5283. doi: [10.1038/sj.emboj.7601400](#)
 23. Chandrasekaran L, He CZ, Al-Barazi H, Kruttsch HC, Iruela-Arispe ML, Roberts DD. Cell contact-dependent activation of alpha3beta1 integrin modulates endothelial cell responses to thrombospondin-1. *Mol Biol Cell*. 2000;11:2885–2900. doi: [10.1091/mbc.11.9.2885](#)
 24. Grant DS, Yenisey C, Rose RW, Tootell M, Santra M, Iozzo RV. Decorin suppresses tumor cell-mediated angiogenesis. *Oncogene*. 2002;21:4765–4777. doi: [10.1038/sj.onc.1205595](#)
 25. Pereira L, Andrikopoulos K, Tian J, Lee SY, Keene DR, Ono R, Reinhardt DP, Sakai LY, Biery NJ, Bunton T, et al. Targeting of the gene encoding fibrillin-1 recapitulates the vascular aspect of Marfan syndrome. *Nat Genet*. 1997;17:218–222. doi: [10.1038/ng1097-218](#)
 26. Kostka G, Giltay R, Bloch W, Addicks K, Timpl R, Fassler R, Chu ML. Perinatal lethality and endothelial cell abnormalities in several vessel compartments of fibulin-1-deficient mice. *Mol Cell Biol*. 2001;21:7025–7034. doi: [10.1128/MCB.21.20.7025-7034.2001](#)
 27. Kim S, Bell K, Mousa SA, Varner JA. Regulation of angiogenesis in vivo by ligation of integrin alpha5beta1 with the central cell-binding domain of fibronectin. *Am J Pathol*. 2000;156:1345–1362. doi: [10.1016/S0002-9440\(10\)65005-5](#)
 28. Nicosia RF, Bonanno E, Smith M. Fibronectin promotes the elongation of microvessels during angiogenesis in vitro. *J Cell Physiol*. 1993;154:654–661. doi: [10.1002/jcp.1041540325](#)
 29. Gonzalez AM, Gonzales M, Herron GS, Nagavarapu U, Hopkinson SB, Tsuruta D, Jones JC. Complex interactions between the laminin alpha 4 subunit and integrins regulate endothelial cell behavior in vitro and angiogenesis in vivo. *Proc Natl Acad Sci U S A*. 2002;99:16075–16080. doi: [10.1073/pnas.252649399](#)
 30. Sharma B, Handler M, Eichstetter I, Whitelock JM, Nugent MA, Iozzo RV. Antisense targeting of perlecan blocks tumor growth and angiogenesis in vivo. *J Clin Invest*. 1998;102:1599–1608. doi: [10.1172/JCI3793](#)
 31. Zagzag D, Shiff B, Jallo GI, Greco MA, Blanco C, Cohen H, Hukin J, Allen JC, Friedlander DR. Tenascin-C promotes microvascular cell migration and phosphorylation of focal adhesion kinase. *Cancer Res*. 2002;62:2660–2668.
 32. Mao JR, Taylor G, Dean WB, Wagner DR, Afzal V, Lotz JC, Rubin EM, Bristow J. Tenascin-X deficiency mimics Ehlers-Danlos syndrome in mice through alteration of collagen deposition. *Nat Genet*. 2002;30:421–425. doi: [10.1038/ng850](#)
 33. Sweeney SM, DiLullo G, Slater SJ, Martinez J, Iozzo RV, Lauer-Fields JL, Fields GB, San Antonio JD. Angiogenesis in collagen I requires alpha2beta1 ligation of a GFP*GER sequence and possibly p38 MAPK activation and focal adhesion disassembly. *J Biol Chem*. 2003;278:30516–30524. doi: [10.1074/jbc.M304237200](#)
 34. Jang YC, Tsou R, Gibran NS, Isik FF. Vitronectin deficiency is associated with increased wound fibrinolysis and decreased microvascular angiogenesis in mice. *Surgery*. 2000;127:696–704. doi: [10.1067/msy.2000.105858](#)
 35. Li R, Luo M, Ren M, Chen N, Xia J, Deng X, Zeng M, Yan K, Luo T, Wu J. Vitronectin regulation of vascular endothelial growth factor-mediated angiogenesis. *J Vasc Res*. 2014;51:110–117. doi: [10.1159/000360085](#)
 36. Brandenberger R, Schmidt A, Linton J, Wang D, Backus C, Denda S, Muller U, Reichardt LF. Identification and characterization of a novel extracellular matrix protein nephronectin that is associated with integrin alpha8beta1 in the embryonic kidney. *J Cell Biol*. 2001;154:447–458. doi: [10.1083/jcb.200103069](#)
 37. Linton JM, Martin GR, Reichardt LF. The ECM protein nephronectin promotes kidney development via integrin alpha8beta1-mediated stimulation of Gdnf expression. *Development*. 2007;134:2501–2509. doi: [10.1242/dev.005033](#)
 38. Al-Hamed MH, Altuwaijri N, Alsahan N, Ali W, Abdulwahab F, Alzahrani F, Majrashi N, Alkuraya FS. A null founder variant in NPNT, encoding nephronectin, causes autosomal recessive renal agenesis. *Clin Genet*. 2022;102:61–65. doi: [10.1111/cge.14128](#)
 39. Fujiwara H, Ferreira M, Donati G, Marciano DK, Linton JM, Sato Y, Hartner A, Sekiguchi K, Reichardt LF, Watt FM. The basement membrane of hair follicle stem cells is a muscle cell niche. *Cell*. 2011;144:577–589. doi: [10.1016/j.cell.2011.01.014](#)
 40. Patra C, Diehl F, Ferrazzi F, van Amerongen MJ, Novoyatleva T, Schaefer L, Muhlfeld C, Jungblut B, Engel FB. Nephronectin regulates atrio-ventricular canal differentiation via Bmp4-Has2 signaling in zebrafish. *Development*. 2011;138:4499–4509. doi: [10.1242/dev.067454](#)
 41. Patra C, Ricciardi F, Engel FB. The functional properties of nephronectin: an adhesion molecule for cardiac tissue engineering. *Biomaterials*. 2012;33:4327–4335. doi: [10.1016/j.biomaterials.2012.03.021](#)
 42. Kuphal S, Wallner S, Bosserhoff AK. Loss of nephronectin promotes tumor progression in malignant melanoma. *Cancer Sci*. 2008;99:229–233. doi: [10.1111/j.1349-7006.2007.00678.x](#)
 43. Fang L, Kahai S, Yang W, He C, Seth A, Peng C, Yang BB. Transforming growth factor-beta inhibits nephronectin-induced osteoblast differentiation. *FEBS Lett*. 2010;584:2877–2882. doi: [10.1016/j.febslet.2010.04.074](#)
 44. Tsai NY, Wang F, Toma K, Yin C, Takatoh J, Pai EL, Wu K, Matcham AC, Yin L, Dang EJ, et al. Trans-seq maps a selective mammalian retinotectal synapse instructed by nephronectin. *Nat Neurosci*. 2022;25:659–674. doi: [10.1038/s41593-022-01068-8](#)
 45. Kuek V, Yang Z, Chim SM, Zhu S, Xu H, Chow ST, Tickner J, Rosen V, Erber W, Li X, et al. NPNT is expressed by osteoblasts and mediates angiogenesis via the activation of extracellular signal-regulated kinase. *Sci Rep*. 2016;6:36210. doi: [10.1038/srep36210](#)
 46. Zhang Y, Wang D, Zhao Z, Liu L, Xia G, Ye T, Chen Y, Xu C, Jin X, Shen C. Nephronectin promotes cardiac repair post myocardial infarction via activating EGFR/JAK2/STAT3 pathway. *Int J Med Sci*. 2022;19:878–892. doi: [10.7150/ijms.71780](#)
 47. Jawoniyi O, Gormley K, McGleenan E, Noble HR. Organ donation and transplantation: awareness and roles of healthcare professionals—a systematic literature review. *J Clin Nurs*. 2018;27:e726–e738. doi: [10.1111/jocn.14154](#)
 48. Esser TU, Roshanbinfar K, Engel FB. Promoting vascularization for tissue engineering constructs: current strategies focusing on HIF-regulating scaffolds. *Expert Opin Biol Ther*. 2019;19:105–118. doi: [10.1080/14712598.2019.1561855](#)
 49. Thurston G, Suri C, Smith K, McClain J, Sato TN, Yancopoulos GD, McDonald DM. Leakage-resistant blood vessels in mice transgenically overexpressing angiopoietin-1. *Science*. 1999;286:2511–2514. doi: [10.1126/science.286.5449.2511](#)
 50. Westerfield M. *The Zebrafish Book: a Guide for the Laboratory Use of Zebrafish (Brachydanio rerio)*. Eugene, OR: University of Oregon Press. 1993.
 51. Ablooglu AJ, Tkachenko E, Kang J, Shattil SJ. Integrin alphaV is necessary for gastrulation movements that regulate vertebrate body asymmetry. *Development*. 2010;137:3449–3458. doi: [10.1242/dev.045310](#)
 52. Baker M, Robinson SD, Lechertier T, Barber PR, Tavora B, D'Amico G, Jones DT, Vojnovic B, Hodivala-Dilke K. Use of the mouse aortic ring assay to study angiogenesis. *Nat Protoc*. 2011;7:89–104. doi: [10.1038/nprot.2011.435](#)
 53. Wakayama Y, Fukuhara S, Ando K, Matsuda M, Mochizuki N. Cdc42 mediates bmp-induced sprouting angiogenesis through Fmn3-driven assembly of endothelial filopodia in zebrafish. *Dev Cell*. 2015;32:109–122. doi: [10.1016/j.devcel.2014.11.024](#)
 54. Schulte-Merker S, Stainier DY. Out with the old, in with the new: reassessing morpholino knockdowns in light of genome editing technology. *Development*. 2014;141:3103–3104. doi: [10.1242/dev.112003](#)
 55. Avraamides CJ, Garmy-Susini B, Varner JA. Integrins in angiogenesis and lymphangiogenesis. *Nat Rev Cancer*. 2008;8:604–617. doi: [10.1038/nrc2353](#)
 56. Sato Y, Uemura T, Morimitsu K, Sato-Nishiuchi R, Manabe R, Takagi J, Yamada M, Sekiguchi K. Molecular basis of the recognition of nephronectin by integrin alpha8beta1. *J Biol Chem*. 2009;284:14524–14536. doi: [10.1074/jbc.M900200200](#)
 57. Ma J, Bi L, Spurlin J, Lwigale P. Nephronectin-integrin alpha8 signaling is required for proper migration of periocular neural crest cells during chick corneal development. *Elife*. 2022;11:11. doi: [10.7554/eLife.74307](#)
 58. Wilson CL, Hung CF, Burkel BM, Ponik SM, Gharib SA, Schnapp LM. Nephronectin is required to maintain right lung lobar separation during embryonic development. *Am J Physiol Lung Cell Mol Physiol*. 2023;324:L335–L344. doi: [10.1152/ajplung.00505.2021](#)

59. Ahnert P, Kirsten H. Association of ITGAV supports a role of angiogenesis in rheumatoid arthritis. *Arthritis Res Ther*. 2007;9:108. doi: [10.1186/ar2313](https://doi.org/10.1186/ar2313)
60. Huang CC, Lawson ND, Weinstein BM, Johnson SL. reg6 is required for branching morphogenesis during blood vessel regeneration in zebrafish caudal fins. *Dev Biol*. 2003;264:263–274. doi: [10.1016/j.ydbio.2003.08.016](https://doi.org/10.1016/j.ydbio.2003.08.016)
61. Howe K, Clark MD, Torroja CF, Torrance J, Berthelot C, Muffato M, Collins JE, Humphray S, McLaren K, Matthews L, et al. The zebrafish reference genome sequence and its relationship to the human genome. *Nature*. 2013;496:498–503. doi: [10.1038/nature12111](https://doi.org/10.1038/nature12111)
62. Gut P, Reischauer S, Stainier DYR, Arnaout R. Little fish, big data: zebrafish as a model for cardiovascular and metabolic disease. *Physiol Rev*. 2017;97:889–938. doi: [10.1152/physrev.00038.2016](https://doi.org/10.1152/physrev.00038.2016)
63. DeCicco-Skinner KL, Henry GH, Cataisson C, Tabib T, Gwilliam JC, Watson NJ, Bullwinkle EM, Falkenburg L, O'Neill RC, Morin A, et al. Endothelial cell tube formation assay for the in vitro study of angiogenesis. *J Vis Exp*. 2014;91:51312. doi: [10.3791/51312](https://doi.org/10.3791/51312)
64. Benjamin LE, Golijanin D, Itin A, Pode D, Keshet E. Selective ablation of immature blood vessels in established human tumors follows vascular endothelial growth factor withdrawal. *J Clin Invest*. 1999;103:159–165. doi: [10.1172/JCI5028](https://doi.org/10.1172/JCI5028)
65. Carpentier G, Berndt S, Ferratge S, Rasband W, Cuendet M, Uzan G, Albanese P. Angiogenesis analyzer for ImageJ—a comparative morphometric analysis of "endothelial tube formation assay" and "fibrin bead assay". *Sci Rep*. 2020;10:11568. doi: [10.1038/s41598-020-67289-8](https://doi.org/10.1038/s41598-020-67289-8)
66. Yokosaki Y, Monis H, Chen J, Sheppard D. Differential effects of the integrins alpha9beta1, alphavbeta3, and alphavbeta6 on cell proliferative responses to tenascin. Roles of the beta subunit extracellular and cytoplasmic domains. *J Biol Chem*. 1996;271:24144–24150. doi: [10.1074/jbc.271.39.24144](https://doi.org/10.1074/jbc.271.39.24144)
67. Rupp PA, Czirok A, Little CD. alphavbeta3 integrin-dependent endothelial cell dynamics in vivo. *Development*. 2004;131:2887–2897. doi: [10.1242/dev.01160](https://doi.org/10.1242/dev.01160)
68. Nikolic I, Stankovic ND, Bicker F, Meister J, Braun H, Awwad K, Baumgart J, Simon K, Thal SC, Patra C, et al. EGFL7 ligates alphavbeta3 integrin to enhance vessel formation. *Blood*. 2013;121:3041–3050. doi: [10.1182/blood-2011-11-394882](https://doi.org/10.1182/blood-2011-11-394882)
69. Chim SM, Tickner J, Chow ST, Kuek V, Guo B, Zhang G, Rosen V, Erber W, Xu J. Angiogenic factors in bone local environment. *Cytokine Growth Factor Rev*. 2013;24:297–310. doi: [10.1016/j.cytogfr.2013.03.008](https://doi.org/10.1016/j.cytogfr.2013.03.008)
70. Kitchen CM, Cowan SL, Long X, Miano JM. Expression and promoter analysis of a highly restricted integrin alpha gene in vascular smooth muscle. *Gene*. 2013;513:82–89. doi: [10.1016/j.gene.2012.10.073](https://doi.org/10.1016/j.gene.2012.10.073)
71. Zhou M, Zhu Y, Zhou Z, Qi F, Zheng S, Gao S, Li Y, Liu Y, Du J. Fibroblast-secreted phosphoprotein 1 mediates extracellular matrix deposition and inhibits smooth muscle cell contractility in Marfan syndrome aortic aneurysm. *J Cardiovasc Transl Res*. 2022;15:959–970. doi: [10.1007/s12265-022-10239-8](https://doi.org/10.1007/s12265-022-10239-8)
72. Warthi G, Faulkner JL, Doja J, Ghanam AR, Gao P, Yang AC, Slivano OJ, Barris CT, Kress TC, Zawieja SD, et al. Generation and comparative analysis of an Itga8-CreER (T2) mouse with preferential activity in vascular smooth muscle cells. *Nat Cardiovasc Res*. 2022;1:1084–1100. doi: [10.1038/s44161-022-00162-1](https://doi.org/10.1038/s44161-022-00162-1)